

This work was written as part of one of the author's official duties as an Employee of the United States Government and is therefore a work of the United States Government. In accordance with 17 U.S.C. 105, no copyright protection is available for such works under U.S. Law.

Public Domain Mark 1.0

<https://creativecommons.org/publicdomain/mark/1.0/>

Access to this work was provided by the University of Maryland, Baltimore County (UMBC) ScholarWorks@UMBC digital repository on the Maryland Shared Open Access (MD-SOAR) platform.

Please provide feedback

Please support the ScholarWorks@UMBC repository by emailing scholarworks-group@umbc.edu and telling us what having access to this work means to you and why it's important to you. Thank you.



RESEARCH ARTICLE

10.1029/2021JD036249

Key Points:

- Goddard Earth Observing System-Version 5 and Community Earth System Model Version 1 predict similar removal timescales of stratospheric smoke injected by megafires
- Removal timescales of smoke with a 2% effective mass fraction of black carbon match observations
- Removal timescales and plume peak heights are sensitive to injection height, loading, and mixing state

Correspondence to:

G. D'Angelo,
gennaro@lanl.gov





Citation:

D'Angelo, G., Guimond, S., Reisner, J., Peterson, D. A., & Dubey, M. (2022). Contrasting stratospheric smoke mass and lifetime from 2017 Canadian and 2019/2020 Australian megafires: Global simulations and satellite observations. *Journal of Geophysical Research: Atmospheres*, 127, e2021JD036249. <https://doi.org/10.1029/2021JD036249>

Received 22 NOV 2021

Accepted 26 APR 2022

Contrasting Stratospheric Smoke Mass and Lifetime From 2017 Canadian and 2019/2020 Australian Megafires: Global Simulations and Satellite Observations

Gennaro D'Angelo¹ , Steve Guimond^{2,3} , Jon Reisner¹ , David A. Peterson⁴, and Manvendra Dubey¹ 

¹Los Alamos National Laboratory, Los Alamos, NM, USA, ²Joint Center for Earth Systems Technology, University of Maryland Baltimore County, Baltimore, MD, USA, ³Department of Physics, University of Maryland Baltimore County, Baltimore, MD, USA, ⁴Naval Research Laboratory, Monterey, CA, USA

Abstract Stratospheric injections of carbonaceous aerosols and combustion gases by extreme wildfires have become increasingly common. Recent “megafires,” particularly large and intense fires, delivered particulate burdens to the lower stratosphere comparable to those of moderate volcanic eruptions. The 2017 Canadian megafire generated four large Pyrocumulonimbi (pyroCbs), injecting up to ≈ 0.3 Tg of smoke in the lower stratosphere. Even more extreme, the 2019/2020 Australian event produced a pyroCb activity resulting in stratospheric smoke intrusions of ≈ 1 Tg. To understand their contrasting behavior, we present global climate simulations of the atmospheric response to these events, applying smoke burdens informed by remote observations. Model outcomes, compared to satellite data of smoke transport, reproduce reasonably well the initial plume rise, at 0.2–0.3 km/day, attaining heights of ≈ 20 km in Canada and above 30 km in Australia. Global dispersal of the plume occurs within about 3 weeks in both cases, consistent with observations. Smoke removal timescales, ≈ 5 months for the Canadian megafire, agree with remote measurements. During the Australian megafire, observations indicate stratospheric injections three times as large, and models predict comparatively longer smoke lifetimes, ≈ 16 months. After the latter event, atmospheric optical depths and radiative cooling achieved values close to those measured following the Pinatubo eruption. Sensitivity tests of model assumptions indicate, in accord with prior studies, that smoke burden, injection heights, and black carbon content can determine plume evolution and possible climate impacts. An empirical relation between peak heights of stratospheric plumes and lifetimes is derived that can help assess megafire impacts on the stratosphere, climate and the Earth system.

1. Introduction¹

Pyrocumulonimbus clouds (pyroCb, Fromm & Servranckx, 2003) generated by intense wildfires (“megafires”) are known to inject large amounts of smoke particulate species in the atmosphere, often well above the troposphere (e.g., Damoah et al., 2006; Fromm et al., 2000; Fromm et al., 2005). Two recent multi-pyroCb events, in the Pacific Northwest (e.g., Peterson et al., 2018) and Australia (New South Wales and Victoria, e.g., Khaykin et al., 2020), resulted in stratospheric aerosol enhancements comparable to those associated with moderate volcanic eruptions (Peterson et al., 2021). Troposphere to stratosphere transport induced by pyroCb activity, however, is not limited to particulate material, but also involves gaseous combustion products, such as CO, H₂O (e.g., Jost et al., 2004; Kablick et al., 2018; Pumphrey et al., 2021), HCN, CH₃CN and CH₃OH (e.g., Schwartz et al., 2020; Simpson et al., 2011), which can lead to secondary aerosol formation (e.g., Yee et al., 2013) and alter global atmospheric composition. Awareness of the stratospheric impact of smoke plume injections has grown over the past decade as megafires have become more frequent (e.g., Jolly et al., 2015; Parks & Abatzoglou, 2020; Westerling, 2016) and observations more extensive. Recently, efforts have intensified to use remote and in situ measurements (e.g., Baars et al., 2019; Ohneiser et al., 2020), along with laboratory studies (e.g., Liu et al., 2020; Murphy et al., 2021), to assist general circulation and Earth system models in predicting possible regional and global effects of these extreme events.

The wildfires that erupted on 12 August 2017 in the Pacific Northwest, between Southern British Columbia and northern Washington State, generated seven, near-concurrent pyroCbs (Fromm et al., 2021). The four most intense were active in British Columbia, hence the term BC17 event. The pyroCbs each lasted for a period between 1 and 4 hr, and were collectively active for about a 5-hr period. Remote observations suggest that the

© 2022. The Authors.

This is an open access article under the terms of the [Creative Commons Attribution-NonCommercial-NoDerivs License](#), which permits use and distribution in any medium, provided the original work is properly cited, the use is non-commercial and no modifications or adaptations are made.

pyroCb activity lifted an estimated 0.1–0.3 Tg of smoke aerosols into the lower stratosphere, an order of magnitude more than any previous amount released by a single-cluster wildfire event (Peterson et al., 2018). It is estimated that each of the BC17 pyroCbs lifted between 0.03 and 0.08 Tg of smoke particles above the troposphere, up to altitudes of ≈ 13 km and at least 1 km into the stratosphere (e.g., Peterson et al., 2018). Although upper troposphere to lower stratosphere infusion of carbonaceous aerosols may have continued for a few to several days via diabatic lofting, after the main pyroCb activity ended (Das et al., 2021; Torres et al., 2020), recent analysis suggests that most of the smoke likely reached the stratosphere during the main pyroCb event, on 12–13 August (Fromm et al., 2021). Measurements of the ultra-violet aerosol index (UVAI) indicate that by August 14 stratospheric smoke covered an estimated area of roughly 800,000 km² over northern Canada (with UVAI values far exceeding 10). By August 17, the smoke plume reached the northern Atlantic Ocean, Europe 2 days later, and encircled the Northern Hemisphere by the end of the month (Khaykin et al., 2018), partly stretching over the tropics (Kloss et al., 2019). Observations by instruments on board the CALIPSO satellite (Winker et al., 2009), which monitors atmospheric aerosol levels, could detect stratospheric smoke for at least 4 months after the BC17 event. These measurements are also confirmed by data from multiple other satellites (Bourassa et al., 2019). Estimates based on measurements by the Limb Profiler (LP) instrument (Chen et al., 2020), flying on board the Suomi National Polar-orbiting Partnership (NPP) satellite, indicate that aerosol extinction profiles returned to pre-event values by June 2018 (Das et al., 2021; Torres et al., 2020). Finally, in situ airborne observations confirmed that thickly coated black carbon (BC) decayed from the stratosphere with an *e*-folding time of ≈ 5 months, providing an independent measure of the smoke removal timescale (J. Schwarz, October 2021, personal communication).

The powerful pyroCb activity resulting from the BC17 event, which had set a new benchmark in terms of atmospheric emissions by wildfires, was soon eclipsed by another, more extreme event in the Southern Hemisphere. A combination of adverse weather conditions in the Southeast region of Australia, which included a multi-year drought spell and unprecedented heat waves (Nolan et al., 2020), led to the 2019/2020 New South Wales and Victoria bushfires. From September 2019 to early January 2020, about 58,000 km² of mostly temperate broad-leaf forest was burned (Boer et al., 2020). Between December 29 and January 4, a very complex system of wildfires generated at least 38 pyroCbs (referred to here, altogether, as the NSWV19/20 event) in two distinct phases, which injected smoke directly into the upper troposphere and lower stratosphere, up to altitudes of ≈ 17.5 km (Khaykin et al., 2020; Peterson et al., 2021). The first and more intense phase was characterized by continuous pyroCb activity that lasted about 45 hr whereas the second, less intense, phase (around January 4) resulted in activity lasting about 6 hr (Peterson et al., 2021). Satellite measurements indicate that the plume rising from the fires produced a stratospheric cloud extending over $\approx 6.1 \times 10^6$ km² (Khaykin et al., 2020). The combined mass of smoke particles, released in the stratosphere, is estimated at 0.3–1.0 Tg, around three times that of the BC17 event (Khaykin et al., 2020; Peterson et al., 2021). Some estimates suggest an even larger mass loading (Hirsch & Koren, 2021). Heating produced via absorption of solar radiation and re-radiation (i.e., emission of thermalized radiation) by the smoke aerosols lofted the plume (Malone et al., 1985) to heights of over 30 km within about 3 months, generating the highest observed layer of particulate material since the eruption of Mount Pinatubo in 1991 (e.g., McCormick et al., 1995; Minnis et al., 1993). Remote measurements suggest that part of the smoke self-organized as anticyclonic vortices (a similar occurrence was found for the 2017 event, Khaykin et al., 2020; Kablick et al., 2020; Lestrelin et al., 2021). Satellite data indicate that the stratospheric aerosol extinction remained 2–3 times higher than background levels well into 2021 (Peterson et al., 2021). The plume also lifted into the stratosphere extremely large amounts of gaseous combustion products, such as CO, CO₂ and H₂O (Kablick et al., 2020; Khaykin et al., 2020; Schwartz et al., 2020; Shiraishi & Hirata, 2021). The smoke plume, spreading eastward, reached South America within about a week (Ohneiser et al., 2020), and covered the entire Southern Hemisphere over the following week (e.g., Hirsch & Koren, 2021; Khaykin et al., 2020).

Several studies have modeled the transport of smoke generated by the Canadian megafire, using either NASA's Goddard Earth Observing System-Version 5 (GEOS5) or NCAR's Community Earth System Model (CESM) (e.g., Christian et al., 2019; Das et al., 2021; Torres et al., 2020; Yu et al., 2019). They found plume lifetimes in the stratosphere ranging from 4.5 to 8 months and maximum altitudes of the plume between ≈ 17 and ≈ 25 km, depending on some specific aspects of the micro-physical description of aerosols and on the parameters applied to model the smoke, mainly initial mass and injection height, composition and optical properties. For example, Christian et al. (2019) did not take into account the radiative response of smoke particles, which can efficiently absorb solar radiation and warm up. To explain observed estimates of the plume lifetime, Yu et al. (2019) invoked a chemically active smoke, in which photo-chemical reactions remove organic material from smoke aerosols

(e.g., by reacting with ozone). The removal process was found to be efficient and could deplete the plume faster than observed. Therefore, the reaction probability had to be chosen accordingly. Das et al. (2021) calculated the radiation budget of the atmosphere and found that the plume caused a zonal cooling at the surface for first couple of months after the emissions. Similarly, Yu et al. (2021) examined the radiative impacts of the smoke plume in the aftermath of the Australian megafire, and they too found surface cooling in the months following the event, along with stratospheric ozone loss at mid-latitudes in the Southern Hemisphere (see also Khaykin et al., 2020; Solomon et al., 2022).

In this work, we perform global climate simulations with both Goddard Earth Observing System-Version 5 (GEOS5) and CESM, following the stratospheric emission of carbonaceous aerosols, black carbon (BC) and organic carbon (OC, e.g., Andreae, 2019), resulting from the pyroCb activities produced the BC17 and NSWV19/20 events. One goal is to compare the initial and long-term plume evolution based on inputs derived from remote observations and informed by laboratory measurements. Another goal is to apply a consistent description of the smoke in the two events, by prescribing the same poorly known quantities, such as OC/BC mass fraction, particle size, and optical properties. Consequences on the parametrization uncertainty are also quantified. Overall, the aim of this study is to assess the reliability of modeling results when using information that can be reasonably constrained by remote, in situ, and laboratory measurements. Furthermore, the contrasting behavior of the two megafire plumes is harnessed to elucidate mechanisms controlling their lifetime, and long-range and long-term impacts.

2. Methods

To examine the atmospheric transport and assess continental and global effects of smoke plumes originating from large wildfires, numerical simulations of the BC17 event were conducted with the NASA Goddard Earth Observing System-Version 5 (GEOS5) model, applied as an atmospheric global climate model, and with the NCAR Community Earth System Model (CESM). The two models were also used to examine the sensitivity of the results to numerical and physical differences in the formulation of radiation-aerosol interactions. Simulations of the NSWV19/20 event were carried out with CESM only.

2.1. GEOS5

NASA GEOS5 is a finite volume Earth system model that solves the hydrostatic (or non-hydrostatic) equations of motion on a cubed sphere grid with a Lagrangian vertical coordinate (Lin, 2004). The dynamic core is coupled to various physical packages (e.g., clouds, radiation, aerosols, turbulence) and is initialized with reanalysis data that incorporate large sets of observations (Rienecker et al., 2008). For this study, only the atmospheric model component is used. We apply the GOCART aerosol model with a focus on the bins representing black carbon (BC) and organic carbon (OC) aerosols. No interactive chemistry model is employed. Simulations with GEOS5 are conducted with an approximate horizontal grid spacing of $1^\circ \times 1^\circ$ and 72 hybrid sigma-pressure vertical layers from the surface to the model top at 0.01 hPa (≈ 80 km).

GEOS5 was used to simulate transport and settling of the smoke plumes associated with the pyroCb activity resulting from the BC17 megafire. Since the pyroCbs are unresolved (and not modeled) at the applied resolution, atmospheric smoke injection follows the approach of Christian et al. (2019), who used uniform smoke distributions with prescribed aerosol loads in the troposphere and stratosphere. This simple prescription for the injection profile of carbonaceous aerosols is justified by the lack of data on the initial development of the plume (within the first few to several hours). Moreover, it allows us to make comparisons with prior work on this event (e.g., Christian et al., 2019; Das et al., 2021; Torres et al., 2020; Yu et al., 2019).

The smoke mass is injected in a single grid column (close to 53.5°N and 123°W , representative of the pyroCb activity in British Columbia) with 0.2 Tg released around a height of about 13.5 km, in the lower stratosphere, and an additional 0.2 Tg uniformly spread in the troposphere. This smoke source is added to the other biomass burning sources included in the GEOS5 emission inventory. The smoke aerosol is assumed to be a mixture of OC and BC, 98% and 2% by mass, respectively. However, since the OC/BC mass partition is uncertain, sensitivity tests were conducted by varying the BC mass fraction in the range from 2% to 6%. The smoke profile is held fixed in the model for a 5-hr period, starting on 12 August 2017 at 19:00 UTC. In GEOS5 simulations, the optical properties of the smoke are computed by treating OC and BC particles as an external mixture, with a mean

Table 1
Reference Profile for the Initial Smoke Emission

Event	BC17		NSWV19/20
	GEOS5	CESM1	CESM1
Location ^a	≈53.5°N ≈123°W	≈53.5°N ≈123°W	≈36°S ≈149°E
Height ^b	13–14 km	13–14 km	14–18 km
Mass ^c	0.2 Tg	0.2 Tg	0.8 Tg
Duration ^d	5 hr	≈1 hr	≈1 hr
BC/OC ^e	0.02	0.02	0.02
Radius ^f	350 nm	300 nm	300 nm

^aApproximate geographical coordinates of smoke emission. ^bAltitude of smoke injection in the stratosphere (varied for sensitivity study). ^cSmoke mass injected in the stratosphere (varied for sensitivity study). ^dDuration of the initial smoke emission. ^eBlack-to-Organic carbon mass ratio in the plume (varied for sensitivity study). ^fMean radius of smoke particles (varied for sensitivity study).

particle radius of 350 nm. We stress that while an external mixture formalism is applied in the model, the effective BC mass fraction intrinsically accounts for uncertainties in physical and chemical properties of smoke particles and their mixing state with organic carbon (which is weakly absorbing).

2.2. CESM1

Community Earth System Model is an Earth system model with fully coupled atmosphere, land, ocean, and sea ice components (Gent et al., 2011; Hurrell et al., 2013). This study uses CESM 1.2 (here referred to as CESM1). The atmosphere configuration is based on the Whole Atmosphere Community Climate Model (WACCM, Marsh et al., 2013), a chemistry climate model that has a resolved stratosphere and extends into the thermosphere up to ≈ 140 km (5×10^{-6} hPa), with a $1.9^\circ \times 2.5^\circ$ horizontal resolution (the same as the land component) and 66 pressure levels. The ocean has a $1^\circ \times 1^\circ$ horizontal resolution (the same as the sea ice component) and 60 levels, down to a depth of ≈ 5 km. The dynamical and radiative interactions of soot particles with the atmosphere are calculated with the Community Aerosol and Radiation Model for Atmospheres module (CARMA, e.g., Mills et al., 2014, and references therein). The initial climate state applied on the

dates of the main pyroCb activity is based on the specifications of the “medium to low emissions” Representative Concentration Pathway (RCP4.5) scenario for the concentrations of greenhouse gases (Meinshausen et al., 2011; Taylor et al., 2012).

The optical properties of OC and BC aerosols used in Whole Atmosphere Community Climate Model (WACCM) derive from the Optical Properties of Aerosols and Clouds database (Hess et al., 1998). In CESM1 simulations, the smoke plumes are assumed to be an internal mixture of OC and BC, with a 2% mass fraction of BC (which, however, remains uncertain). The effective optical properties of the mixture are computed according to the prescription of Chylek et al. (2019), who proposed an average of OC and BC complex refractive indices weighted by the volume fraction of the species (OC is weakly absorbing, implicitly including contributions from brown carbon). In the simulations, smoke particles do not undergo surface chemistry changes (aging) or coagulation, and only evolve through transport and deposition. These simple approximations on the nature of the smoke particles are dictated by the large uncertainties on the properties of freshly emitted smoke, and on its evolution and changing composition by cooling, cloud processing, and photo-chemistry. As in GEOS5, the effective BC mass fraction is also intended to account for some of these uncertainties.

The initial distribution of the smoke plumes applied in the simulations is as described in Section 2.1 for the BC17 event (see also Section 4.1). In both models, the vertical resolution near the tropopause is ≈ 1 km, similar to that applied in other studies (e.g., Das et al., 2021; Torres et al., 2020; Yu et al., 2019). CESM1 simulations were also used to gauge the sensitivity of the stratospheric dynamics of the smoke and its removal timescale on the amount of particles injected in the stratosphere (0.05–0.6 Tg), the stratospheric injection height (≈ 10–14 km), and particle radius (100–350 nm). For the NSWV19/20 event (≈ 36°S and ≈ 149°E), the smoke mass injected in the stratosphere (≈ 14–18 km) is in the range 0.7–1.0 Tg (Khaykin et al., 2020; Peterson et al., 2021) and the particle radius is 300 nm (see also Section 4.2). The two main outbreaks, at the end of December 2019 and at the beginning of January 2020, were grouped in a single emission event. A summary of the initial smoke emission profile and particle properties is reported in Table 1. As for GEOS5 simulations, in all cases the initial stratospheric smoke burden represents half of the total smoke mass released in the atmosphere, with the other half uniformly distributed in the troposphere.

3. Data

3.1. Satellite Observations

In order to validate model calculations, we use data from space-borne instruments, which provide high-resolution information on the vertical distribution of aerosols. The data include radiation back-scatter (from Cloud-Aerosol

Lidar with Orthogonal Polarization, CALIOP) and extinction measurements (from SAGE III-ISS and OMPS-LP). These instruments are briefly reviewed here.

The Cloud-Aerosol Lidar with Orthogonal Polarization (CALIOP), flown on board NASA's polar-orbiting CALIPSO satellite (Stephens et al., 2002; Winker et al., 2003), records measurements of polarization sensitive/insensitive attenuated radiation, at wavelengths of 532 and 1,064 nm (Winker et al., 2009). The instrument performs global profiling of aerosols and clouds in the troposphere and stratosphere, up to altitudes of 40 km (532 nm channel) and up to 30 km (1,064 nm channel) above sea level. Data sampling is performed at a vertical resolution of 30–60 m and at a horizontal resolution of 335 m (Winker et al., 2009). Cloud-Aerosol Lidar with Orthogonal Polarization (CALIOP) data can determine the height of cloud and aerosol layers and discriminate between them (Z. Liu et al., 2009), based on statistical differences of their optical and physical properties (Z. Liu et al., 2004). Aerosol layers can then be classified and characterized by means of pre-defined types (Kim et al., 2018; Omar et al., 2005, 2009).

The Stratospheric Aerosol and Gas Experiment III (SAGE III) is a NASA instrument, built as part of the Earth Observing System program, installed on the International Space Station (SAGE III-ISS, Cisewski et al., 2014; Knepp et al., 2020). The instrument is a spectrometer that measures near-UV, visible, and near-Infrared (IR) radiation through the Earth's limb during solar and lunar occultations and limb scattering (during the daytime side of the orbit). SAGE III-ISS provides measurements of the vertical distribution of aerosols from the upper troposphere through the stratosphere, and of ozone from the upper troposphere through the mesosphere. The instrument also performs high vertical resolution measurements of trace gases, such as water vapor and NO₂ (Flittner et al., 2018). The spectrometer provides continuous spectral coverage between 290 and 1,030 nm. Additional aerosol measurements are provided at a wavelength of 1,550 nm.

The Limb Profiler (LP) is one of the spectrometers of the Ozone Mapping and Profiler Suite (OMPS), flying on board the NASA/National Oceanic and Atmospheric Administration Suomi National Polar-orbiting Partnership satellite. The near real-time Ozone Mapping and Profiler Suite (OMPS) data products (based on limb-scattering measurements) include total ozone column density, total NO₂ column density, vertical ozone concentration, and vertical aerosol profiles from the tropopause up to altitudes of 60 km (Rault & Loughman, 2013; Taha et al., 2021). The instrument operates in the wavelength range between 290 and 1,000 nm, with a vertical sampling of about 1–1.5 km (Jaross et al., 2014). Single-wavelength measurements can be used to retrieve aerosol extinction as a function of height (e.g., Chen et al., 2018; Loughman et al., 2018; Taha et al., 2021).

Comparison studies of aerosol extinction measurements have shown that the agreement between CALIPSO and SAGE III-ISS sensors is about 25% in the latitude band 30°S–30°N, but agreement deteriorates outside this range (Kar et al., 2019). Similar (or somewhat better) levels of agreement have been found from comparisons of measurements acquired by Ozone Mapping and Profiler Suite (OMPS)-LP and SAGE III-ISS instruments (Taha et al., 2021).

3.2. Smoke Properties

The BC mass fraction, morphology, and mixing state, which largely determine the smoke optical properties (e.g., absorption cross-section and single-scattering albedo), depend on fuel type, combustion phase, and atmospheric processing by moisture and photo-chemistry. For example, flaming fires produce much more BC than smoldering fires, and cloud and/or ice processing can compact freshly emitted BC (which is fractal) and render it less absorbing. Organics can condense onto BC particulate, forming transparent coatings that enhance its absorption cross-section. These micro-physical processes result in large uncertainties in the properties of smoke particles, which we do not attempt to treat in detail but rather to evaluate with sensitivity tests, informed by laboratory and field measurements of fire smoke emissions and aged plumes.

The BC/OC mass fraction in fresh smoke can vary by an order of magnitude, from less than 1% for smoldering fires to over 10% for flaming fires, as shown in laboratory studies (Adachi et al., 2019; Romonosky et al., 2019). The mixing state, determined by fuel composition, distribution, moisture and fire dynamics, is highly variable and complex. Ambient fire plumes (primarily warm tropospheric plumes) have been sampled over a range of ages and they start out with mean mass fractions of around 2% (Lee et al., 2020). Recent analysis of pyroCbs indicates that secondary organic aerosol formation, by condensation in cold updrafts of organic vapors (co-emitted by fires), can reduce the BC mass fraction to about 1% as the plume rises toward the upper troposphere and lower

stratosphere (Ditas et al., 2018). In addition, in situ airborne measurements in the upper troposphere provide evidence of thick coatings (≥ 150 nm on BC cores ≈ 70 nm in radius, Ditas et al., 2018) on BC particles emitted by biomass burning (see also Dählkötter et al., 2014), and of extremely thick coatings (≥ 250 nm) in the BC17 plume sampled in the lower stratosphere (J. Katich, October 2021, personal communication). Organic coatings on BC cores can enhance light absorption by lensing (S. Liu et al., 2014; Lee et al., 2020), but the effect depends strongly on morphology (Cappa et al., 2012) and can be reduced by extruded structures. Moreover, the absorption enhancement does not increase linearly with coating thickness but it saturates at about twice the core size (Lack & Cappa, 2010) and can drop for extremely thick coatings (>3 times the core size), typical of the BC17 smoke injection. Additionally, laboratory and field observations show that fresh BC is a fractal structure with high mass absorption cross-section, which collapses to a compact spherical structure after cloud processing with a much lower absorption cross-section (Bhandari et al., 2019).

The non-linear effects of BC core morphology and coating thickness on absorption of radiation are complex, variable and uncertain. We therefore use the aforementioned findings and follow recent simulations of the BC17 plume, which required smoke composition 1.5%–2.5% BC in mass to reproduce the observed plume rise and transport (e.g., Christian et al., 2019; Das et al., 2021; Torres et al., 2020; Yu et al., 2019).

4. Results

Observational evidence indicates that the formation of pyroCb clouds is aided by particular weather conditions, such as high surface winds, relatively dry and unstable near-surface air, and moist air on top of the dry layer. These conditions tend to generate large-scale air cells rising in the middle and upper troposphere (Peterson et al., 2017). Thermal buoyancy resulting from the heat released by large and intense wildfires can accentuate this vertical motion, providing a direct channel for smoke particles and other aerosols and combustion gases to penetrate the lower stratosphere. However, the initial dynamics of pyroCb formation and lofting of smoke plumes cannot be captured by global atmospheric models, such as those employed in this study. Within the applied spacial scales, these processes are unresolved. Therefore, the initialization of the smoke plume is necessarily idealized and based on bulk quantities that can be constrained by remote measurements (e.g., the estimated smoke mass). This simplification is mainly intended to represent a mean-field injection after the pyroCb activity has ceased. For the current purposes, we follow the general approach of Christian et al. (2019), who also modeled the BC17 event. Similar approximations were applied by, for example, Yu et al. (2019), Torres et al. (2020), and Das et al. (2021).

Except for the initial smoke injection profile, which resulted in a significantly greater stratospheric burden following the NSWV19/20 event, the same approximations are applied in the two scenarios. The physical, compositional, and optical properties of the smoke particles are also the same. Although somewhat different fuel types were burned in the fires (e.g., boreal vs. temperate/eucalyptus forest), it is assumed that corrections due to differences in the aerosol properties do not substantially affect transport and settling of smoke (compared to, e.g., mass loading and injection heights).

4.1. Models of the BC17 Event

Christian et al. (2019) argued that, since smoke plumes mix during their initial ascent, the choice of the vertical emission profile is not very important as long as the heights at which most of the burden is injected are reasonably accurate. They assumed that the smoke column released 0.2 Tg of carbonaceous aerosols around a height of 13.5 km, based on the emission analysis of Peterson et al. (2018), and uniformly distributed an equal amount of particles between this layer and the surface. In this regard, it should be noted that the CALIPSO satellite passed over the region about 8 hr after the pyroCb activity had ended. Thus, the initial injection profile also represents a time average (over the first many hours) of the smoke emissions. Christian et al. (2019) also modeled carbonaceous aerosols as composed of BC and OC, in a 6/94 mass ratio. This is in line with near-field aircraft observations, revealing that sub-micron aerosols emitted by wildfires are overwhelmingly composed of organic matter (e.g., Garofalo et al., 2019). As a comparison, Yu et al. (2019) inferred an initial smoke mass injection of 0.3 Tg of aerosols, emitted between 12 and 13 km, with a mass partition of 2/98 between BC and OC. In their study, Torres et al. (2020) applied an emission profile that injected 0.3 Tg of smoke particles (BC/OC), 2.5% BC by mass, between 10 and 12 km (see also Das et al., 2021).

An accurate micro-physical model of a smoke plume, involving coagulation of the particulate material and growth via chemical reactions with ambient and other emitted gases, is outside the scope of this study. These processes not only are technically challenging but also largely unconstrained. In fact, the chemical evolution and optical characteristics of stratospheric smoke emitted by pyroCbs remains highly uncertain. Instead, as in other published studies, we aim at capturing averaged properties of the smoke plume, as it rises from the injection site and disperses through the atmosphere, eventually depositing the particulate material to the surface.

Diabatic lofting of a smoke plume is driven by solar radiation absorbed by the particles entrained in the local air mass. This process mostly depends on three quantities: the absorption coefficient of the particles, their radius, and the particles' concentration (which is set by the atmospheric burden). Black carbon can absorb radiation very efficiently, from the ultra-violet (UV) side to the IR side of the spectrum (e.g., Bergstrom et al., 2002). Organic carbon also represents a significant absorbing species in the ultra-violet (UV), but not so much at longer wavelengths. Nonetheless, as mentioned above, the particulate mixture is predominantly composed of OC that can include some brown carbon, whose contribution to absorption can therefore be non-negligible. Absorption and re-radiation of a particle mixture also depends on the total surface area of the particles, that is, on the number density which, for a given particulate mass per unit volume, is larger for smaller particles. Therefore, self-lofting of a smoke plume is enhanced by the presence of small particles, which also take longer to sediment. Near-field measurements indicate that freshly emitted BC particles in pyroCb plumes become readily coated with organics and, over a period of 24–48 hr, the particles grow 10 times or more in mass, reaching hundreds of nano-meters in radius (Dahlkötter et al., 2014; Ditas et al., 2018). The choice of the particle size used in the models also reflects these observations (see also Murphy et al., 2021).

The initial horizontal transport of the BC17 smoke plume is illustrated in the left panels of Figure 1, for the reference emission profile, 5 (top), 10, and 20 (bottom) days after injection. The mixing ratio of the smoke-to-air mass is integrated through the atmospheric column. In agreement with observations, the smoke traveled past Nova Scotia and over the northern Atlantic Ocean in about 5 days, and over Europe within a week (e.g., Khaykin et al., 2018; Peterson et al., 2018). The model indicates that it took about 3 weeks for the smoke to encircle the entire Northern Hemisphere, also in accord with the transport of aerosol clouds produced by volcanic eruptions (e.g., McCormick & Veiga, 1992; Stowe et al., 1992). The optical depths of the smoke column is reported on the right, and displays a similar distribution pattern as in the left panels, as expected. Lidar observations, acquired over Southern France toward the end of August, measured optical depths values averaging around 0.1 (Khaykin et al., 2018), consistent with the model.

In the days following the event, the smoke plume was observed to rise in the stratosphere, reaching altitudes of ≈ 19 – 20 km after about 20 days (≈ 0.3 km/day, Peterson et al., 2018). The left panels of Figure 2 show this initial lofting phase as obtained from the models, GEOS5 (top) and CESM1 (bottom). The smoke-to-air mass mixing ratio plotted in the top panels is averaged horizontally in the latitude band 40°N – 80°N , whereas the average is performed over the entire globe in the bottom panels. The nominal altitude of the tropopause near the latitude of the event is ≈ 12 km. In both simulations, the smoke has a 2% BC mass fraction and applies the reference emission profile (see also Section 2.1). The initial rise in the GEOS5 model is somewhat faster than in the CESM1 model but both are in reasonable accord with observations, resulting in maximum aerosol concentrations in the plume at heights around 19–20 km after 3 weeks. The faster initial rise in GEOS5 may be related to the more horizontally localized injection source (Das et al., 2021). The panels also include CALIOP data of the relative attenuated scattering ratios, in which pre-event background values are close to 1. After the event, the scattering ratios increased up to 30% relative to the background. The purple contours in the panels mark values of the ratio ≥ 1.14 , tracking dense parts of the smoke layers. The dark blue line segment represents a linear fit to the maximum scattering ratios in the CALIOP scattering time series. The smoke rise in the models during the first week is also in good agreement with OMPS-LP measurements of the mean aerosol extinction (see Das et al., 2021).

As the plume rises and disperses in the stratosphere, the aerosol number density decreases and so does diabatic lofting to higher altitudes, which is also hindered by gravitational settling in low-density air (Stenke et al., 2013). Consequently, the plume height stabilizes, as sedimentation reduces the aerosol burden. This process can be seen in the right panels of Figure 2, which show the vertical evolution of the plume over a period of 8 months. During this time, the heights reached by smoke particulate in the stratosphere agrees reasonably well with SAGE III-ISS aerosol extinction observations (Yu et al., 2019), represented by gray symbols with error bars. The extinction coefficients are sampled at a wavelength of 1,020 nm and the reference extinction value used to define the plume

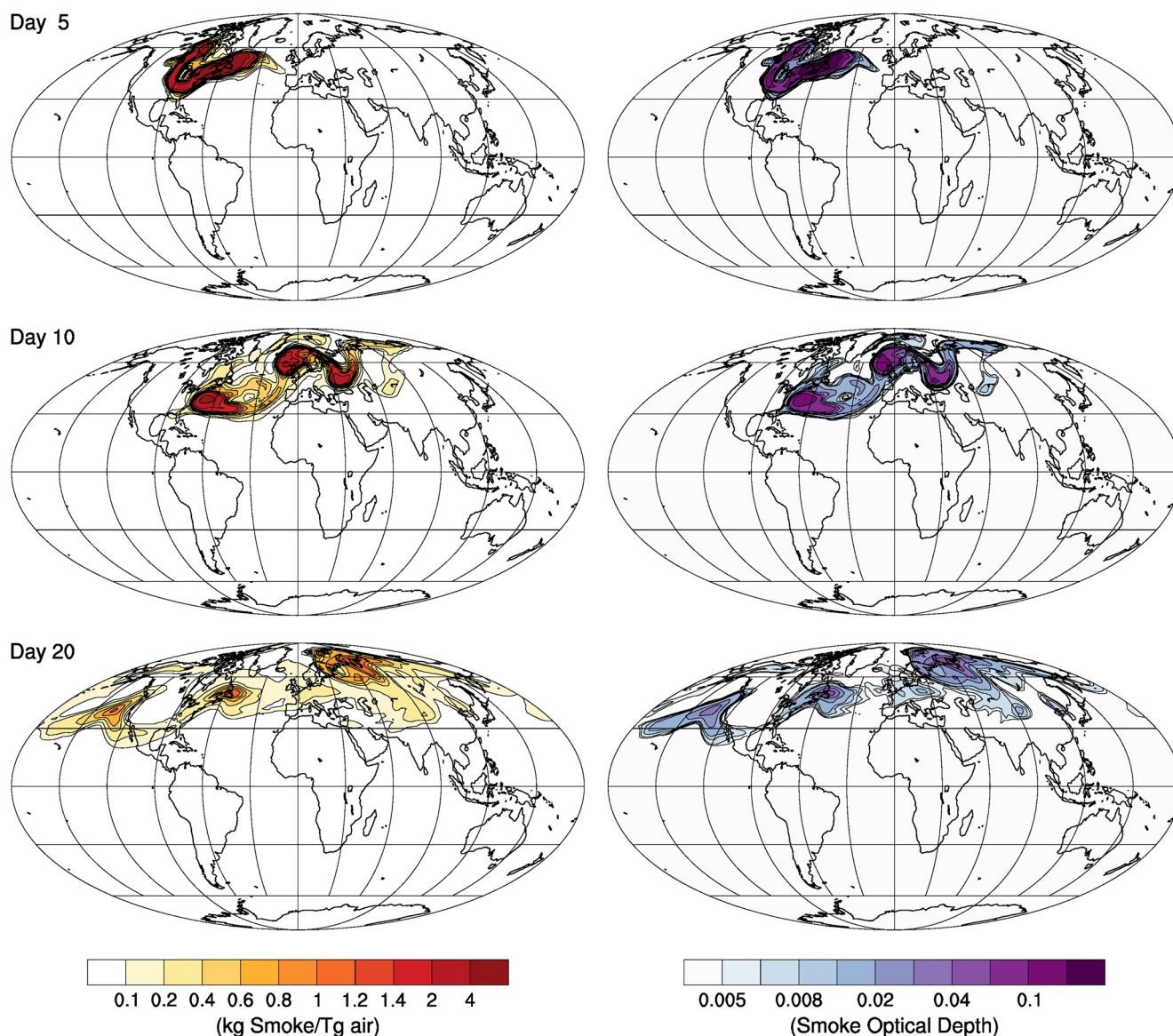


Figure 1. Left: Smoke-to-air mass-mixing ratio, column-integrated over the whole atmosphere, as a function of latitude and longitude for the CESM1 simulation with the default smoke injection profile (see Section 2.1), with a 2% black carbon mass ratio and particles of radius 300 nm. Right: Cumulative optical depth (OD) of the smoke column. From top to bottom, the maps display the global atmospheric dispersion of the plume 5, 10, and 20 days after the BC17 event (as indicated).

height is $1.5 \times 10^{-4} \text{ km}^{-1}$. These measurements also indicate that the plume rose somewhat above 20 km after about 2 months. For comparison, the plume ejected by the 2019 Raikoke eruption also ascended by $\approx 7 \text{ km}$ in a 2-month period (Chouza et al., 2020).

Near-field observations indicate that the mass partition of smoke particles (between BC and OC) rapidly changes as the plume rises from the ground. The initial smoke may contain 1%–10% in BC, but particles become readily coated with organics and, as the plume cools while rising toward the upper troposphere and into the stratosphere, the BC fraction can become lower than 1%–2% (Ditas et al., 2018). Secondary organic aerosol formation may further reduce the BC fraction. Sensitivity experiments conducted with GEOS5, imposing a smoke composition with a higher BC mass fraction, 6%, resulted in the plume lofting to heights of about 23–24 km, approximately 5 km higher than in the model with 2% BC shown in Figure 2. In the models, the effective BC mass fraction can be also used as a proxy to capture the net effects of some processes unresolvable at coarse scale. Overall, these results are consistent with those of Yu et al. (2019) and Das et al. (2021), who explored the effects on plume rise of a similar range of smoke compositions.

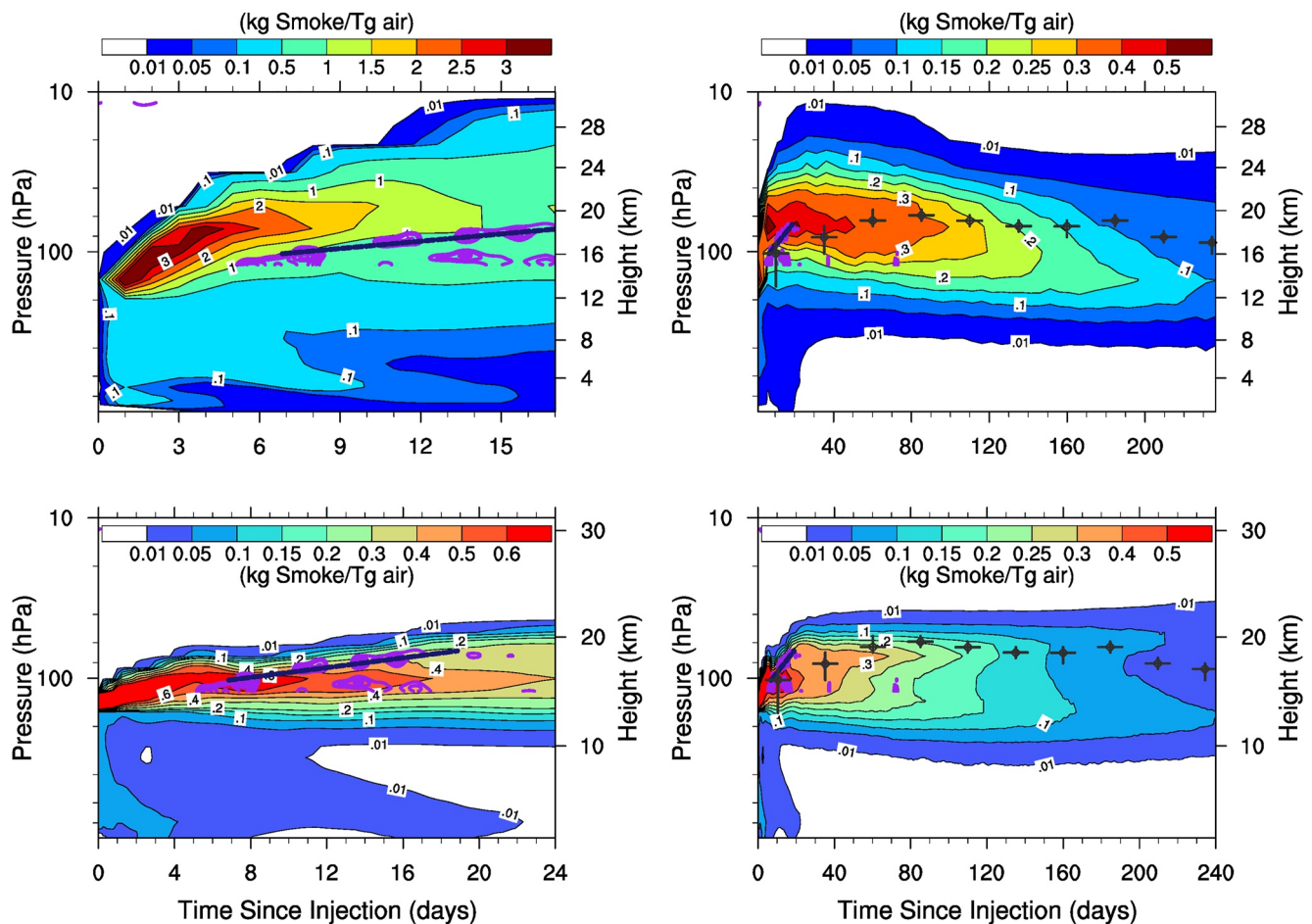


Figure 2. Smoke-to-air mass-mixing ratio, averaged in latitude and longitude (see text for details), as a function of pressure/height and time. (top) GEOS5 simulation of a plume with a 2% black carbon by mass. (bottom) CSM1 simulation for the default smoke injection profile (see Section 2.1) with particles' radii of 300 nm. Left and right panels show, respectively, the rise of the plume and its longer-term evolution. The purple contours (and blue line segment) represent CALIOP data whereas the gray symbols are SAGE III-ISS data (see Section 3).

CALIOP scattering ratios remained above background levels throughout the end of the year, indicating that significant amounts of smoke aerosols persisted in the lower stratosphere for months (Peterson et al., 2018). Aerosol extinction measurements suggest that the stratospheric smoke burden returned to pre-event levels about 10 months after the pyroCb activity (Torres et al., 2020). The evolution of the stratospheric smoke mass versus time is shown in Figure 3, for both GEOS5 and CSM1 models. The smoke mass is normalized to the total atmospheric injection. A measure of the mean lifetime of the stratospheric smoke is typically associated to an e -folding decay timescale, that is, when the smoke mass has reduced to $1/e$, about 37%, of its initial value. The introduction of this removal timescale, however, does not imply that the stratospheric burden decays exponentially. For a 2% BC smoke composition, GEOS5 and CSM1 models result in similar smoke lifetimes, at 5.5 months. A three-fold increase in the BC mass fraction (to 6%) can extend the smoke lifetime to ≈ 7 months (compare dashed curves in Figure 3). A comparable removal time of 5 months was obtained by Christian et al. (2019). Yu et al. (2019) also reported an e -folding time of 5 months, although they invoked reduced order photo-chemistry to remove organic material from the plume. Without this loss mechanism, the timescale increases to approximately 8 months. It should be noted that the initial stratospheric burden applied by Yu et al. (2019) was 0.3 Tg and, with the same smoke loading, we obtain a similar removal timescale (see left panel of Figure 4). Torres et al. (2020) and Das et al. (2021) argued that troposphere to stratosphere transport of smoke continued after the initial pyroCb activity via diabatic lofting. To account for the continued infusion of carbonaceous aerosols into the stratosphere, they used an injection profile that effectively smeared emissions between about 9 and 13 km, which resulted in an e -folding removal time of ≈ 5 months (Das et al., 2021). The consistency with our results is not surprising

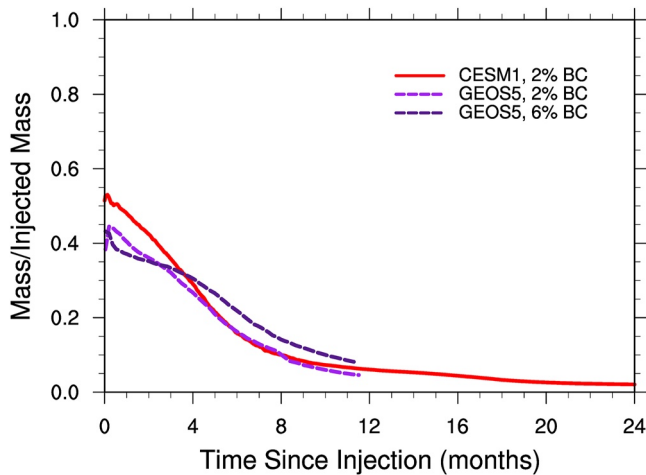


Figure 3. Comparison of the stratospheric smoke removal in CESM1 and GEOS5 simulations, as indicated. The smoke mass integrated at heights above ≈ 13 km is normalized by the total injected mass (0.4 Tg, half of which is injected in the stratosphere). The e -folding removal timescale is between 5 and 6 months in both models for plumes with a 2% black carbon mass fraction. For a higher, 6% BC mass fraction, the removal timescale increases to about 7 months.

since the injection profiles applied herein do extend into the troposphere (see Section 2.1) and, therefore, account to some extent for this additional source of stratospheric aerosols.

To first order, the injection heights of the bulk of the stratospheric smoke determine the fate of the plume. For example, if smoke is only injected just beneath the stratosphere, these (and similar) models do not reproduce the observed features of the plume evolution (e.g., Christian et al., 2019). Indeed, experiments performed with CESM1, based on injection profiles emitting particles around and below the tropopause (at heights $\lesssim 12$ km and reported in Figure 5), indicate that the plume does not rise high enough into the stratosphere. Smoke concentrations in the Figure show that the plume remains below measurements (compare with CALIOP scattering ratios represented by purple contours, the same data as in Figure 2). Nonetheless, diabatic lofting of the plume in the weeks following the emission can still induce transport of some smoke across the tropopause, as can be seen in both panels of Figure 5. Smoke removal (e -folding) timescales in the stratosphere, however, drop to about 1 month (left) and 1.5 months (right), significantly shorter than observational estimates. It should be noted that lofting by solar heating depends on how radiation is attenuated as it passes through (and is absorbed by) the smoke layers. Therefore, the more solar radiation is absorbed in the stratosphere the less is available to drive upward transport of aerosols from the troposphere (see, e.g., solid line in Figure 3).

Another important quantity required by models to provide a reasonable description of the smoke plume evolution is the amount of particulate material injected into the stratosphere. Current estimates place the smoke burden caused by the BC17 event in the 0.1–0.3 Tg mass range (Peterson et al., 2018). CESM1 models using smoke loads in this range are presented in the left panel of Figure 4. The red solid and dashed lines refer to the model with reference emission, in which the solid line represents the total atmospheric smoke mass (column-integrated from the ground upward). The shaded plot encompasses the variation obtained from the models with different stratospheric mass loads (the total initial load is always twice as the stratospheric load). In terms of smoke lifetimes (e -folding timescale) the effect of mass loading is non-linear, resulting in a 10% reduction, relative to the reference case, at the low end and in $\approx 17\%$ increase at the high end.

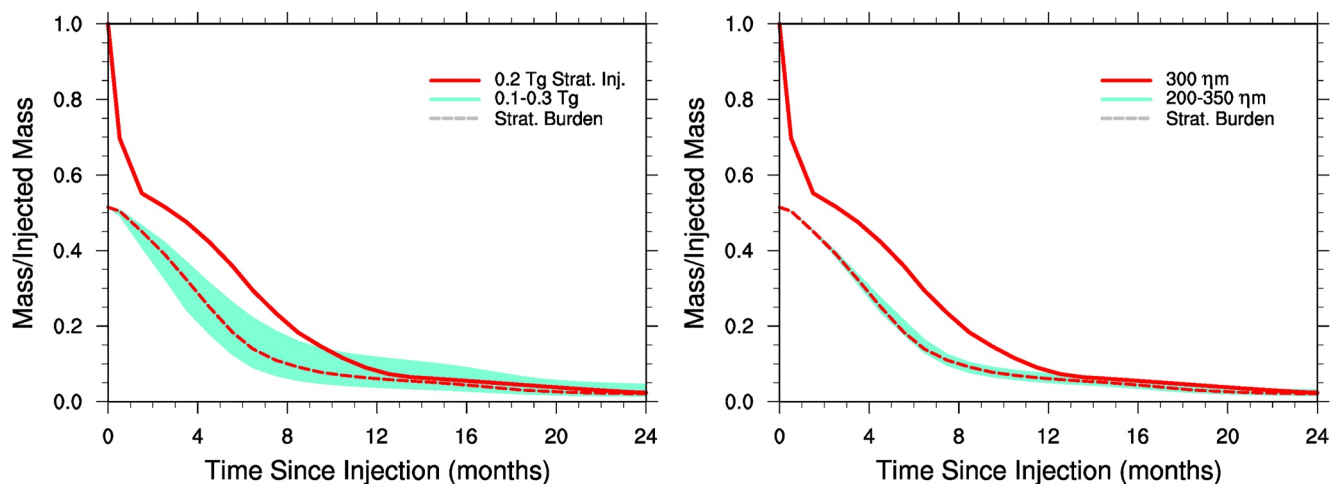


Figure 4. CESM1 simulations with plumes of smoke particles of different mass loads (left) and of different radii (right). The black carbon mass fraction is 2% in all cases. The total, column-integrated smoke mass (solid line) is normalized by the total injected mass (0.2–0.6 Tg). The stratospheric smoke (normalized) mass is also shown (dashed lines). The shaded area indicates the variation of the stratospheric smoke removal time for the applied smoke loads and particle radii. The e -folding timescale varies by over 3 months on the left and by less than a month on the right. Model data are monthly-averaged.

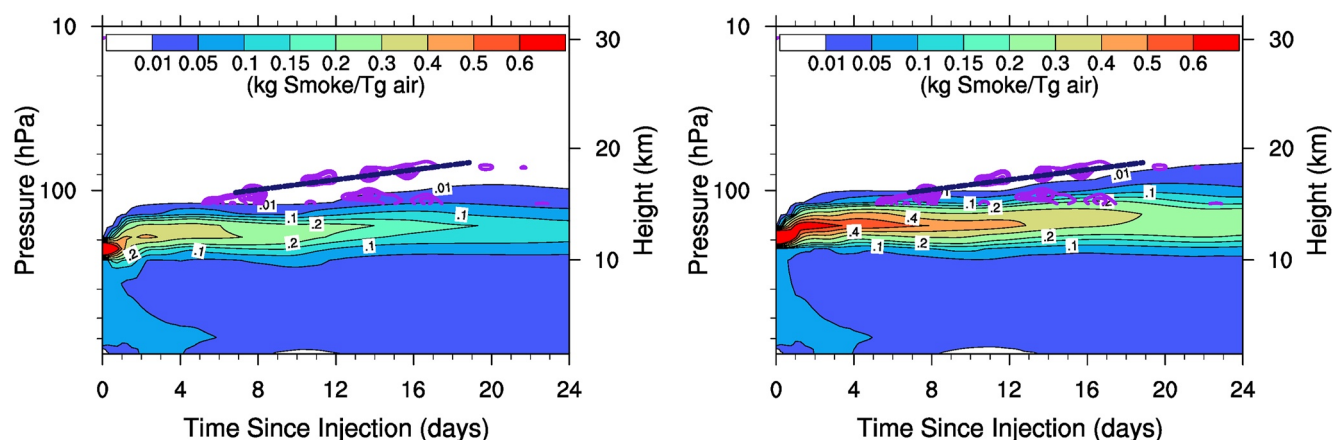


Figure 5. Average smoke-to-air mass-mixing ratio versus height and time, as in Figure 2, but for smoke emission profiles injecting 0.2 Tg of particulate around altitudes of ≈ 10.5 km (left) and ≈ 11.5 km (right). Additional 0.2 Tg of smoke are uniformly distributed in the layers underneath in both cases. The purple contours and blue line segment represent CALIOP back-scatter data (the same as in Figure 2). The line segment tracks maximum scattering ratios in the CALIOP scattering time series.

The sensitivity of the stratospheric smoke removal on the mean particle radius was also tested, in a range up to 350 nm. Smaller particles, that is, higher number densities, are expected to enhance the cumulative light absorption (and re-emission in the IR spectrum) of the smoke because of a larger exposed surface. Hence, heating is expected to increase. Smaller mass also implies lower settling velocities and longer residence times. The right panel of Figure 4 shows models based on the reference injection profile and various particle sizes. The difference between cases with a reference radius of 300 nm and with a radius of 350 nm is marginal. A plume composed of smaller, 200 nm-radius particles does allow for a longer residence times in the stratosphere, but by less than a month. As mentioned above, rising smoke aerosols grow to these sizes. Nonetheless, experiments applying particle radii of 100 nm also result in lifetimes shorter than 7 months. Overall, from these tests it appears that the uncertainties on the smoke burden and heights of injection account for most of the uncertainty on the lifetime of the stratospheric smoke and the duration of associated climate impacts.

Estimates of the plume peak heights and stratospheric smoke lifetime can help assess the possible consequences of megafires on the stratosphere and the Earth system. To provide such estimates, additional experiments were carried out with CESM1, in which the initial injection height of the stratospheric smoke was between 13 and 14 km (as in the reference emission profile, see Section 2.1) and between 12 and 13 km, and varying the initial smoke mass in the plume. Otherwise, the models are the same as those discussed above. Results are presented in Figure 6, which shows on the left a relation between the maximum height of the smoke plume and the e -folding time. The plume height is calculated based on the optical depth (OD) of the smoke integrated from the top of the model atmosphere downward, for three threshold values of OD, as indicated. The altitudes of the initial stratospheric emissions are rendered by different colors. The smoke mass injected in the stratosphere in each model is also reported. The right panel shows how the e -folding time varies as a function of the initial mass of stratospheric smoke. The peak height of the plume for the reference optical depth of ≈ 0.01 is also indicated for each model. Comparing the cases at the two injection heights, the smoke lifetime can grow by a factor of ≈ 2 for a 1–2 km increase in emission altitude. However, additional experiments not reported here suggest that this trend may slow down as the altitude of injection is increased further. The plume peak heights show a similar, factor ≈ 2 difference. For a smoke burden of 0.2 Tg initially emitted, Figures 5 and 6 indicate that the e -folding time grows by a factor of more than five over the considered range of injection heights (mostly due to the short residence times following tropospheric injections, see Figure 5). Restricting to the results shown in Figure 6, for equal smoke burdens at the beginning, plume peak altitudes reach between 20% and 50% higher in the higher-altitude emission scenario, and the removal timescale is typically twice as long. A six-fold increase in the injected smoke mass causes a 50% (lower-altitude emission) or 80% increase in peak heights, and a factor of ≈ 3 extension in smoke lifetimes.

The radiative and thermal impacts of stratospheric aerosols depend on particle-radiation interactions and on the residence time of the particulate. They have been studied in particular detail for volcanic plumes, even those produced by moderate eruptions (see, e.g., Wang et al., 2013; Jégou et al., 2013; Bègue et al., 2017, and

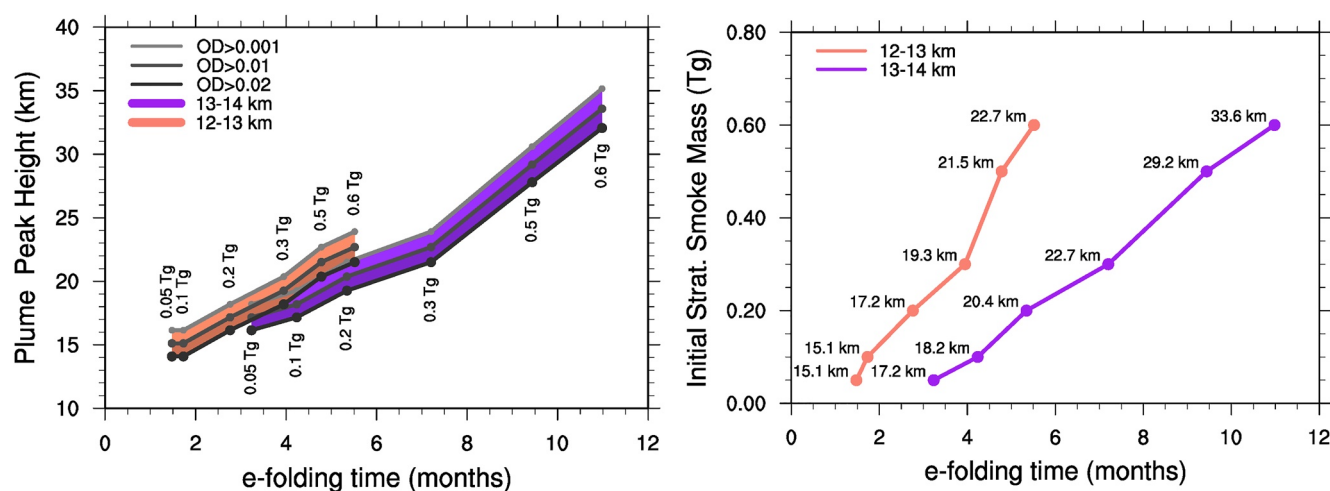


Figure 6. Left: Peak height of smoke plumes versus (e -folding) removal timescale in the stratosphere. The smoke optical depth (OD) is integrated from the top of the model atmosphere downward. The two sets of models refer to initial emission profiles in which the stratospheric smoke is injected into different layers, between 12 and 13 km (orange shades) and between 13 and 14 km (purple shades), as indicated. Models also differ by the initial smoke mass injected in the stratosphere, whose value is indicated above/below the shaded region. Other model assumptions are the same as for the reference emission scenario discussed in the text. Right: Variation of the e -folding time versus initial smoke mass injected in the stratosphere for the models represented in the left panel. The plume peak height at OD \approx 0.01 is also indicated for each model.

references therein). Past work on volcanic emissions also highlighted that stratospheric aerosol lifetimes depend on the altitudes of injection, the same behavior as that of smoke emissions. To place results illustrated in Figure 6 into context, some estimates may be helpful. Volcanic plumes detected between heights of \approx 15 and \approx 20 km have been associated with e -folding removal timescales of 5–8 months (e.g., Bluth et al., 1997, and references therein). But shorter removal timescales, around 3 months, have also been reported (e.g., Bègue et al., 2017; Jégou et al., 2013). For plume heights extending above 25 km, caused by more powerful eruptions, removal timescales can reach or exceed 1 year (e.g., Baran & Foot, 1994; Bluth et al., 1997).

4.2. Models of the NSWV19/20 Event

The 2019/2020 bushfires in Southeast Australia represented a very complex event in terms of pyroCb activity and can be divided in two main phases, the first and more intense occurring on December 29–31, 2019, and the second occurring on 4 January 2020. By intensity and emissions, the latter phase alone was comparable to the BC17 event. Nonetheless, for simplicity in model setup, the smoke emission profile generated by the combined pyroCb activity is approximated in a manner similar to that described in the previous sections, and it is intended to describe the cumulative emission of the two phases of pyroCb activity. Clearly, this simplification can affect the initial rise of the plume. The smoke mass is released in the stratosphere between heights of \approx 14 and \approx 18 km (see also Table 1), applying burdens between 0.7 and 1.0 Tg (Khaykin et al., 2020; Peterson et al., 2021). This is at least a three-fold increase relative to the 2017 megafire in British Columbia. As for the BC17 event, an equal amount of smoke mass is uniformly distributed in the layers underneath (down to the ground). Aerosol particles are assumed to be an internal mixture of OC and BC, 98% and 2% by mass respectively, and have radii of 300 nm. Smoke burdens of approximately 1 Tg were also used by Yu et al. (2021) to model this event. However, they applied a slightly larger BC to OC mass ratio and injected the particles at somewhat lower altitudes.

In situ lidar observations indicate that the smoke plume traveled eastward and reached Southern Chile within about a week (Ohneiser et al., 2020). Over a period of about 2 weeks the fastest patches of smoke had returned over Australia (Hirsch & Koren, 2021; Khaykin et al., 2020). By February 2020, smoke had also spread to Antarctica (Yu et al., 2021). These timescales for the horizontal transport are reproduced fairly well by the CESM1 model displayed in Figure 7. The left panels shows the smoke concentration, integrated through the atmospheric column, one (top), two, and four weeks (bottom) after the emission of 0.8 Tg of particulate material in the stratosphere (see reference values in Table 1). Models also predict some smoke intrusions in the Northern

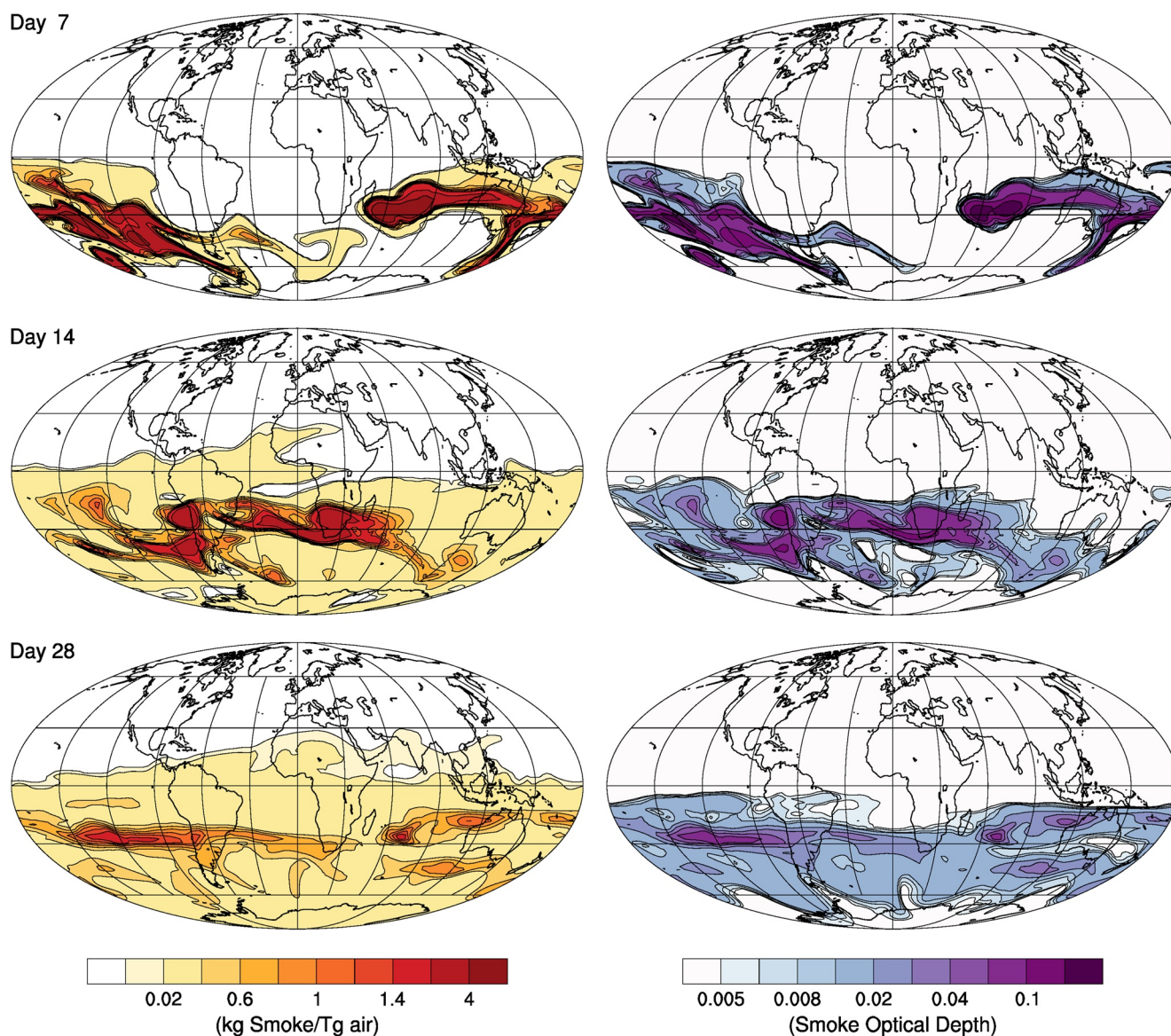


Figure 7. Left: Smoke-to-air mass-mixing ratio, column-integrated over the atmosphere, as a function of latitude and longitude for a CESM1 model for a representation of the NSWV19/20 event, injecting 0.8 Tg of smoke particles in the stratosphere (see Section 4.2). Right: Cumulative optical depth of the smoke column. From top to bottom, the maps display the global atmospheric dispersion of the plume 7, 14, and 28 days after the event, as indicated.

Hemisphere, although this transport is difficult to ascertain from observations given the relative small amounts and the local levels of stratospheric aerosol emissions from volcanic sources in that year (Yu et al., 2021).

The right panels in Figure 7 represent the aerosol optical depths of the smoke column (i.e., integrated throughout the atmosphere). By the second half of January, aerosol optical depths reached ≈ 0.2 (Ohneiser et al., 2020), in accord with the model. Observations also indicate that, during the first few months after the event, the observed perturbation in aerosol optical depth in the stratosphere, up to ≈ 0.01 (at 750 nm and zonally averaged between 20°S and 80°S), matched that caused by the volcanic plume generated by the Raikoke eruption (Khaykin et al., 2020). These optical depth perturbations are also in reasonable agreement with estimates from the model in Figure 7. As a reference, the values of the aerosol optical depths measured after the eruption of Mount Pinatubo peaked at 0.4 (Valero & Pilewskie, 1992) and global averages remained above 0.1 for 2 years (Self et al., 1998).

The smoke plume rose quickly via diabatic lofting, over the first month, slowing down afterward (as aerosols became more diluted in the air). After 3 months, the plume had risen from its injection heights at ≈ 14 –18 km to

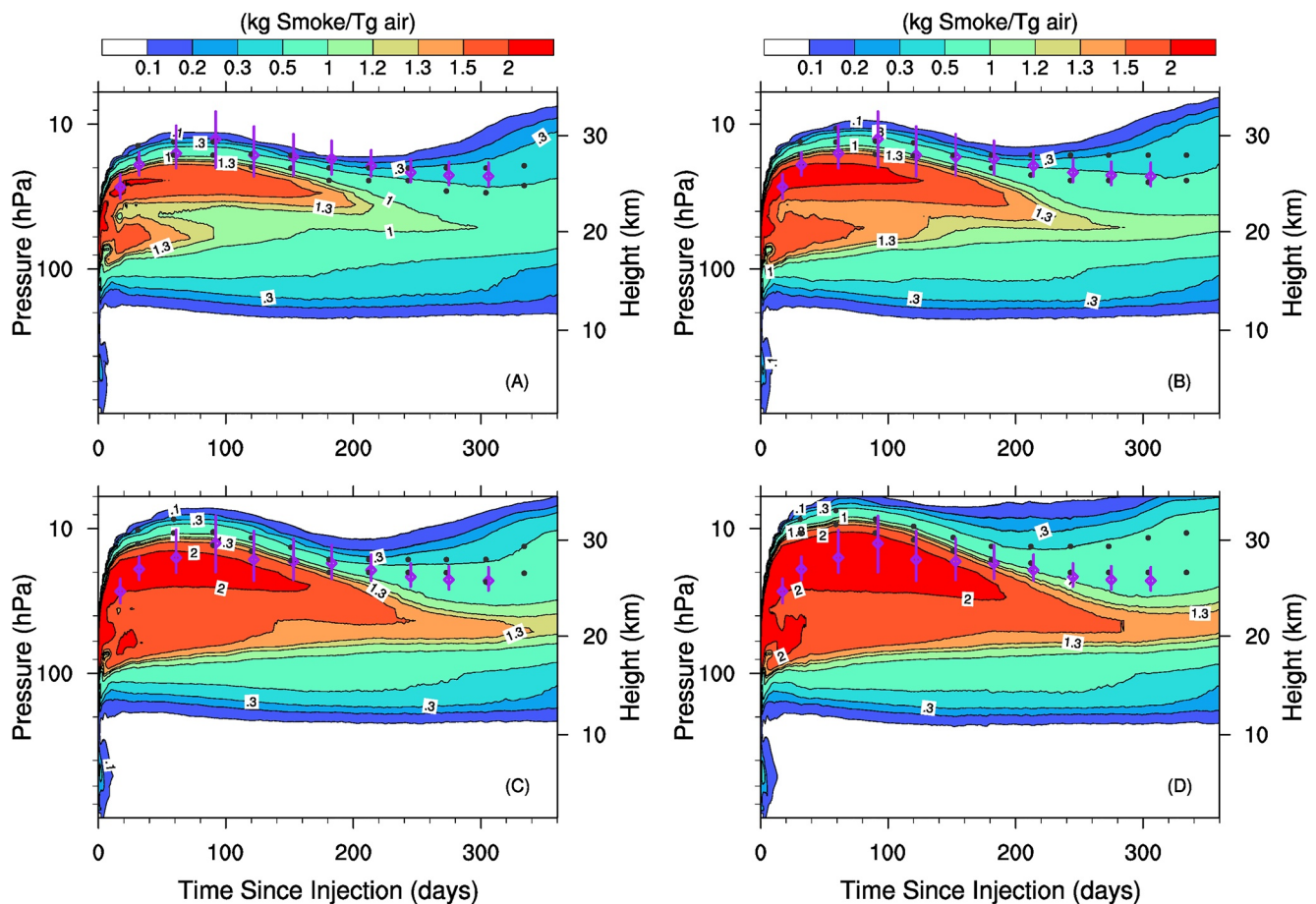


Figure 8. Smoke-to-air mass-mixing ratio, globally averaged in latitude and longitude, as a function of pressure/height and time, obtained from CESM1 simulations of the NSWV19/20 event (particles have 2% black carbon by mass and a radius of 300 nm). The cases represent stratospheric smoke injections of 0.7 Tg (a), 0.8 Tg (b), 0.9 Tg (c) and 1 Tg (d). Equal amounts of smoke particles are injected in the troposphere. The purple symbols are derived from OMPS-LP aerosol extinction data at 997 nm (see Section 3). For given dates, each pair of gray circles represents aerosol extinction levels obtained from the models (see text for details).

above 30 km (Khaykin et al., 2020; Peterson et al., 2021). Figure 8 shows the average evolution of model plumes during the first year, as they rise after injection of 0.7–1 Tg of smoke particles in the stratosphere (see Figure's caption and Table 1 for further details). OMPS-LP aerosol extinction data (see Section 3) are also plotted, represented by purple symbols with error bars. Given the complexity of the event and the simplifying assumptions applied to aerosol emissions in the models, it is expected that the initial plume development can differ from model predictions. Nonetheless, the plume rise over the first month, tracked via CALIOP attenuated scattering ratios (Khaykin et al., 2020), is in good agreement with the OMPS-LP extinction data presented in the Figure, reaching up to ≈ 20 km by January 7, up to ≈ 22 km by the second week of January and above 25 km by the end of the month.

Observational data indicate that the extinction coefficients increased, relative to pre-event background values, by four times during the first 3–4 months following the event. The OMPS-LP extinction coefficients reported in Figure 8, represented purple symbols, are sampled at a wavelength of 997 nm and the error bar covers the extinction range up to $\approx 5 \times 10^{-5} \text{ km}^{-1}$. The gray circles in the Figure indicate the aerosol extinction obtained from the models. At a given date, the upper and lower symbols refer to values of $\approx 5 \times 10^{-5}$ and $\approx 10^{-4} \text{ km}^{-1}$, respectively. It should be noted, though, that the model extinction is averaged over a broad band, including visible wavelengths. Of the models shown in Figure 8, those with 0.7–0.8 Tg of stratospheric injection appear to best capture the initial rise rate and lofting of the smoke over the first 3 months (at $\approx 0.2 \text{ km/day}$), and subsequent plume stabilization.

The stratospheric aerosol extinction remained elevated, 2–3 times higher than background values for at least 10 months after the initial smoke injection. During that time, the extinction coefficient of the atmospheric layers

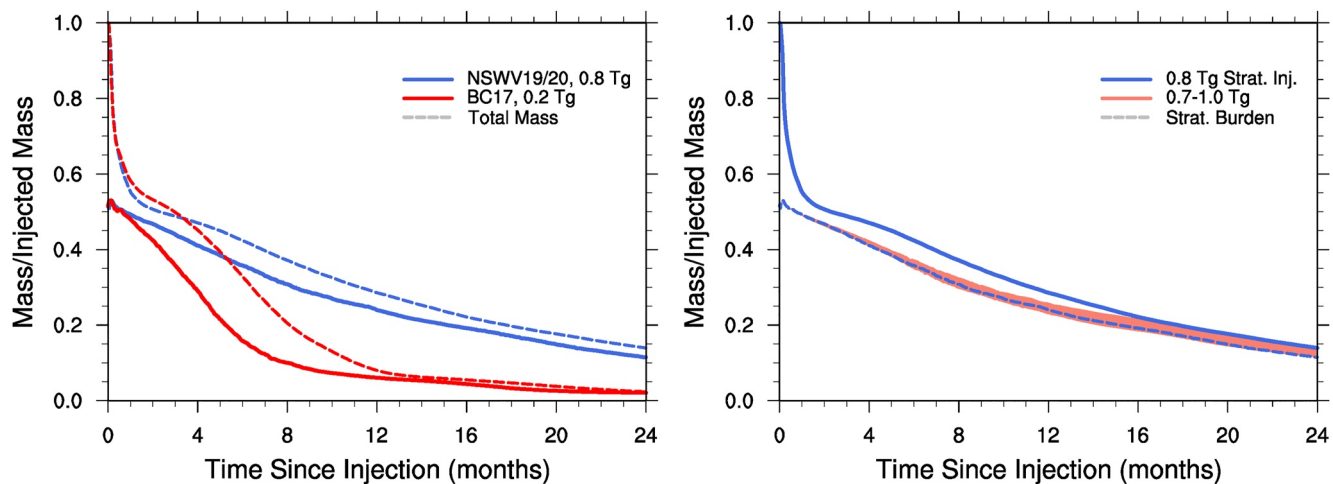


Figure 9. Smoke removal timescales in CESM1 models of the NSWV19/20 event. Left: Comparison of the total (dashed curve) and stratospheric burden (solid curve) between models of the BC17 and NSWV19/20 events (initial stratospheric burden as indicated). The smoke mass is normalized by the total injected mass (twice the stratospheric burden). The e -folding timescale is about 16 months in the NSWV19/20 model, three times that of the BC17 model. Right: Variations of the smoke removal timescale (shaded area) for models of the NSWV19/20 event with a range of initial stratospheric injections (as indicated).

above ≈ 20 km was estimated from OMPS-LP data at values $2 \times 10^{-4} \text{ km}^{-1}$. A smoke layer with an extinction coefficient of $\approx 10^{-4} \text{ km}^{-1}$ persisted around heights of ≈ 25 km at least through the end of the year (Peterson et al., 2021). Figure 9 displays the evolution of the atmospheric and stratospheric smoke burdens in models of the NSWV19/20 event. The left panel compares the evolution of a scenario with a 0.8 Tg initial (stratospheric) burden to the BC17 scenario with reference emission profile (0.2 Tg initial injection, see Table 1). The e -folding removal timescale is ≈ 16 months in the NSWV19/20 model about three times as long as that of the BC17 simulation, despite the initial mass loading being four times as large. As mention above, self-lofting depends on the propagation of solar radiation through the aerosol layers and ensuing attenuation, therefore shadowing tends to reduce its efficacy. The right panel of Figure 9 shows results from experiments with different initial smoke burdens, as indicated. The shaded area encompasses the stratospheric smoke removal timescales. For a 25% increase of the initial aerosol burden (from 0.8 to 1 Tg), the e -folding timescale increases by $\approx 15\%$.

The exceptionally large amount of carbonaceous aerosols emitted in the atmosphere produced a significant radiative response in the aftermath of the NSWV19/20 event. Observations suggest that in the latitude band between $\approx 20^\circ\text{S}$ and 60°S , on average, the solar radiation flux at the surface lowered by about 3 W/m^2 in February (Hirsch & Koren, 2021; Khaykin et al., 2020). The amplitude of the anomaly declined in the following months but remained observable until about June.

To gauge mean zonal anomalies of near-surface temperatures and solar radiation flux at surface caused by smoke emissions and ensuing plume transport, a control and a perturbed ensemble were constructed with CESM1. The control (ten-member) ensemble is used to quantify the reference state (without smoke emissions) of the atmosphere and the internal (stochastic) variability of the model, and was generated by applying a small random perturbation to the atmospheric temperature (see Kay et al., 2015, for details). The perturbed state was determined through a forced (nine-member) ensemble that includes emission scenarios with initial stratospheric injections between 0.8 and 1.0 Tg of smoke and height of injection varying in the range between ≈ 13 and ≈ 18 km (and equal amounts of smoke emitted in lower layers). This latter ensemble is intended to account, to some extent, for observational uncertainties on aerosol emissions. Anomalies are plotted in Figure 10, for the quantities spatially averaged in latitude between 20°S and 60°S . Mean temperature anomalies (solid line) are within -0.2 and 0.1 K , whereas mean surface flux anomalies are within about -3.5 and 2 W/m^2 . The gray shaded region represents the range of stochastic variability of the control ensemble while the colored shaded region provides a measure of the combined uncertainty on the anomaly. In the first 6 months after the event, temperature anomalies points to cooling at values of (negative) 0.1 – 0.2 K (see also Fasullo et al., 2021). During the same period, the radiative forcing perturbation reaches a minimum (i.e., a maximum in magnitude) in February, at about -3 W/m^2 , in agreement with observational assessments (Khaykin et al., 2020). At later times, mean anomalies become comparable

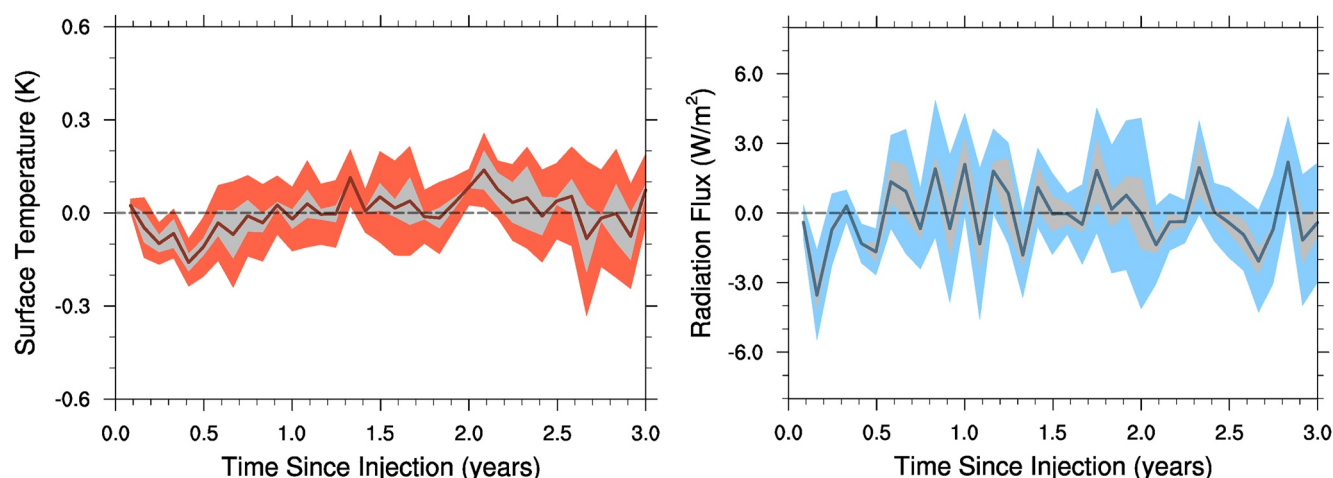


Figure 10. Mean anomalies, averaged in latitude between 20°S and 60°S, of the near-surface atmospheric temperature (left) and net solar radiation flux at surface (right). The means (solid lines) are calculated from ensembles of control (unforced) simulations and various NSWV19/20 emission scenarios (see text for details) using monthly averaged data. The shaded regions represent the standard deviation of the control ensemble (gray) and of both ensembles (colored).

to, or smaller than, the amplitude of the uncertainty, also consistent with remote observations (e.g., Hirsch & Koren, 2021). For comparison, in August 1991, 2 months after Mount Pinatubo eruption, the net solar flux at surface lowered by $\approx 4 \text{ W/m}^2$, zonally averaged between 40°N and 40°S (Minnis et al., 1993). Globally, during the past three decades, volcanic emissions of sulphate aerosols were estimated to be responsible for an average radiative forcing anomaly of approximately -0.1 W/m^2 (Ge et al., 2016; Schallock et al., 2021; Schmidt et al., 2018).

5. Conclusions

The increasing occurrence of megafires, particularly large and intense wildfires, over the past decade demands attention. Recent events include that in British Columbia (2017), Canada, and that in New South Wales and Victoria (2019/2020), Australia. The pyroCb activity generated by these two megafires outclassed any prior such event. Emission of carbonaceous aerosols directly in the upper troposphere and lower stratosphere reached levels typically only associated to those of moderate volcanic eruptions. Likewise, the emission of combustion gases, such as CO, CO₂ and H₂O, was also unprecedented. Remote observations by space-borne instruments have provided ample evidence that these events can induce large, hemispheric scale perturbations in the stratosphere, altering its aerosol and gaseous composition, as well as its radiative balance and circulation for prolonged periods of time. Recently, efforts have intensified to use general circulation and Earth system models to make predictions of large-scale and long-term effects in the aftermath of these events.

We simulated the global atmospheric evolution of the smoke plumes emitted by BC17 and NSWV19/20 scenarios, using GEOS5 and CESM1. The pyroCb activity is assisted by distinct weather conditions which, however, are not resolved or captured by our models. Instead, simulations rely on initial injection of aerosols guided by observational assessments of the smoke burden released in the stratosphere and observed injection heights (based on radiation back-scatter and aerosol extinction profiles). Stratospheric burdens around 0.2 Tg, injected at altitudes of 13–14 km, were estimated for the BC17 event and 0.8–1.0 Tg, released at 14–18 km, for the NSWV19/20 event. A relatively simple micro-physical description of the smoke aerosols is adopted, using a mono-disperse distribution of particles in the range 200–350 nm and a mixture of BC/OC, 2%–6% BC by mass. This choice is broadly supported by laboratory experiments and near-field measurements.

Even though the bulk of the stratospheric injection of smoke particulate in the models is driven by pyroCb activity, diabatic lofting can transport smoke particulate from the upper troposphere to the stratosphere if solar radiation can efficiently penetrate through the upper smoke layers. This latter process is accounted for in the models by applying emission profiles that also inject smoke particles beneath the tropopause. Although many (and often uncertain) details of particle-radiation interactions are not fully captured by these models, the use of distinct aerosol treatments accounts for some of the uncertainties.

The models reproduce the main features of the smoke horizontal transport across the Northern (BC17) and Southern Hemisphere (NSWV19/20), with a global coverage achieved over a period of two to 3 weeks (see Figures 1 and 7). Atmospheric optical depths increased to levels measured after moderate volcanic eruptions. The initial rise of the model plumes, at rates of $\approx 0.2\text{--}0.3$ km/day, agree with observations and so do maximum smoke heights (≈ 20 km after the BC17 event and above 30 km after the NSWV19/20 event, see Figures 2 and 8). The long-term removal of stratospheric smoke is also in accord with observational estimates of ≈ 5 months after the 2017 Canadian megafire (see Figure 3). After the NSWV19/20 event, smoke persisted in the stratosphere for more than 15 months. The modeled removal timescale is ≈ 16 months (see Figure 9).

Although details such as particle sizes and BC/OC partition of the smoke can affect model results, initial stratospheric smoke burden and injection heights broadly characterize the plume evolution. At latitudes comparable to those of the BC17 event, an increase in injection height from ≈ 12.5 to ≈ 13.5 km can lead to differences in maximum plume altitudes of a few to many kilometers, depending on the initial smoke burden. Smoke removal timescales increase with both plume maximum altitude and smoke initial burden (see Figure 6). The broad consistency across different models, applying different micro-physical descriptions for the carbonaceous aerosols and their interactions with radiation and the atmosphere, make predictions on plume rise and dispersal in the aftermath of megafires relatively robust. However, since the initial pyroCb activity may be too difficult to capture by Earth system models, the availability of in situ and remote observations are key to reliable model predictions.

The NSWV19/20 event attained levels of moderate volcanic eruptions not only for the amount of particulate pollution of the stratosphere it generated but also for the climatic response it triggered. In accord with observations, models predict regional cooling in the Southern Hemisphere, peaking in February 2020, when the net solar flux at surface lowered on average by ≈ 3 W/m². Surface temperatures lowered by 0.1–0.2 K (see Figure 10). Even after such a large event, predictions on global metrics spanning many months in the future may be complicated to disentangle from the stochastic variability of the system response and from other injection sources. Nonetheless, sustained monitoring and analysis of megafires is critical to assess and quantify zonal and global atmospheric impacts caused by smoke emissions in Earth system models.

Data Availability Statement

Cloud-Aerosol Lidar with Orthogonal Polarization data plotted in Figures 2 and 5 are included in Peterson et al. (2017). SAGE III-ISS data plotted in Figure 2 are included in Yu et al. (2019). OMPS-LP data plotted in Figure 8 are included in Peterson et al. (2021). Model data to reproduce the Figures included herein can be found at <https://doi.org/10.6084/m9.figshare.17056145> (D'Angelo et al., 2021). NASA Goddard Earth Observing System model is available at https://gmao.gsfc.nasa.gov/GEOS_systems/. NCAR CESM is available at <https://www.cesm.ucar.edu/>.

Acknowledgments

We thank two anonymous reviewers whose comments and suggestions helped improve this paper. We are indebted to Charles (Chuck) Bardeen for kindly providing assistance with the Community Aerosol and Radiation Model for Atmospheres (CARMA) module of CESM1. Steve Guimond thanks members of the NASA/GSFC GMAO for answering questions on the GEOS5 model. This research is supported by the Los Alamos National Laboratory (LANL) Laboratory Directed Research and Development program. David Peterson was supported by the NRL Base Program. Computing resources for this project were provided by the High-Performance Computing Division and Institutional Computing at LANL.

References

- Adachi, K., Sedlacek, A. J., Kleinman, L., Springston, S. R., Wang, J., Chand, D., et al. (2019). Spherical tarball particles form through rapid chemical and physical changes of organic matter in biomass-burning smoke. *Proceedings of the National Academy of Sciences*, 116(39), 19336–19341. <https://doi.org/10.1073/pnas.1900129116>
- Andreae, M. O. (2019). Emission of trace gases and aerosols from biomass burning – An updated assessment. *Atmospheric Chemistry and Physics*, 19(13), 8523–8546. <https://doi.org/10.5194/acp-19-8523-2019>
- Baars, H., Ansmann, A., Ohneiser, K., Haarig, M., Engelmann, R., Althausen, D., et al. (2019). The unprecedented 2017–2018 stratospheric smoke event: Decay phase and aerosol properties observed with the EARLINET. *Atmospheric Chemistry and Physics*, 19(23), 15183–15198. <https://doi.org/10.5194/acp-19-15183-2019>
- Baran, A. J., & Foot, J. S. (1994). New application of the operational sounder HIRS in determining a climatology of sulphuric acid aerosol from the Pinatubo eruption. *Journal of Geophysical Research*, 99(D12), 25673–25679. <https://doi.org/10.1029/94JD02044>
- Bègue, N., Vignelles, D., Berthet, G., Portafaix, T., Payen, G., Jégou, F., et al. (2017). Long-range transport of stratospheric aerosols in the Southern Hemisphere following the 2015 Calbuco eruption. *Atmospheric Chemistry and Physics*, 17(24), 15019–15036. <https://doi.org/10.5194/acp-17-15019-2017>
- Bergstrom, R. W., Russell, P. B., & Hignett, P. (2002). Wavelength dependence of the absorption of black carbon particles: Predictions and results from the TARFOX experiment and implications for the aerosol single scattering albedo. *Journal of the Atmospheric Sciences*, 59(3), 567–577. [https://doi.org/10.1175/1520-0469\(2002\)059<0567:WDOTAO>2.0.CO;2](https://doi.org/10.1175/1520-0469(2002)059<0567:WDOTAO>2.0.CO;2)
- Bhandari, J., China, S., Chandrakar, K. K., Kinney, G., Cantrell, W., Shaw, R. A., et al. (2019). Extensive soot compaction by cloud processing from laboratory and field observations. *Scientific Reports*, 9(1), 11824. <https://doi.org/10.1038/s41598-019-48143-y>
- Bluth, G. J. S., Rose, W. L., Sprod, I. E., & Krueger, A. J. (1997). Stratospheric loading of sulfur from explosive volcanic eruptions. *The Journal of Geology*, 105(6), 671–684. <https://doi.org/10.1086/515972>

- Boer, M. M., Resco de Dios, V., & Bradstock, R. A. (2020). Unprecedented burn area of Australian mega forest fires. *Nature Climate Change*, 10(3), 171–172. <https://doi.org/10.1038/s41558-020-0716-1>
- Bourassa, A. E., Rieger, L. A., Zawada, D. J., Khaykin, S., Thomason, L. W., & Degenstein, D. A. (2019). Satellite limb observations of unprecedented forest fire aerosol in the stratosphere. *Journal of Geophysical Research*, 124(16), 9510–9519. <https://doi.org/10.1029/2019JD030607>
- Cappa, C. D., Onasch, T. B., Massoli, P., Worsnop, D. R., Bates, T. S., Cross, E. S., et al. (2012). Radiative absorption enhancements due to the mixing state of atmospheric black carbon. *Science*, 337(6098), 1078–1081. <https://doi.org/10.1126/science.1223447>
- Chen, Z., Bhartia, P. K., Loughman, R., Colarco, P., & DeLand, M. (2018). Improvement of stratospheric aerosol extinction retrieval from OMPS/LP using a new aerosol model. *Atmospheric Measurement Techniques*, 11(12), 6495–6509. <https://doi.org/10.5194/amt-11-6495-2018>
- Chen, Z., Bhartia, P. K., Torres, O., Jaross, G., Loughman, R., DeLand, M., et al. (2020). Evaluation of the OMPS/LP stratospheric aerosol extinction product using SAGE III/ISS observations. *Atmospheric Measurement Techniques*, 13(6), 3471–3485. <https://doi.org/10.5194/amt-13-3471-2020>
- Chouza, F., Leblanc, T., Barnes, J., Brewer, M., Wang, P., & Koon, D. (2020). Long-term (1999–2019) variability of stratospheric aerosol over Mauna Loa, Hawaii, as seen by two co-located lidars and satellite measurements. *Atmospheric Chemistry and Physics*, 20(11), 6821–6839. <https://doi.org/10.5194/acp-20-6821-2020>
- Christian, K., Wang, J., Ge, C., Peterson, D., Hyer, E., Yorks, J., & McGill, M. (2019). Radiative forcing and stratospheric warming of pyrocumulonimbus smoke aerosols: First modeling results with multisensor (epic, calipso, and cats) views from space. *Geophysical Research Letters*, 46(16), 10061–10071. <https://doi.org/10.1029/2019GL082360>
- Chylek, P., Lee, J. E., Romonosky, D. E., Gallo, F., Lou, S., Shrivastava, M., et al. (2019). Mie scattering captures observed optical properties of ambient biomass burning plumes assuming uniform black, brown, and organic carbon mixtures. *Journal of Geophysical Research: Atmospheres*, 124(21), 11406–11427. <https://doi.org/10.1029/2019JD031224>
- Cisewski, M., Zawodny, J., Gasbarre, J., Eckman, R., Topiwala, N., Rodriguez-Alvarez, O., & Hall, S. (2014). The stratospheric aerosol and gas experiment (SAGE III) on the international space station (ISS) mission. In R. Meynart, S. P. Neeck, & H. Shimoda (Eds.), *Sensors, Systems, and next-generation Satellites xviii* (Vol. 9241, p. 924107). <https://doi.org/10.1117/12.2073131>
- Dahlkötter, F., Gysel, M., Sauer, D., Minikin, A., Baumann, R., Seifert, P., et al. (2014). The Pagami Creek smoke plume after long-range transport to the upper troposphere over Europe - Aerosol properties and black carbon mixing state. *Atmospheric Chemistry and Physics*, 14(12), 6111–6137. <https://doi.org/10.5194/acp-14-6111-2014>
- Damoah, R., Spichtinger, N., Servranckx, R., Fromm, M. D., Eloranta, E. W., Razenkov, I. A., et al. (2006). A case study of pyro-convection using transport model and remote sensing data. *Atmospheric Chemistry and Physics*, 6(1), 173–185. <https://doi.org/10.5194/acp-6-173-2006>
- D'Angelo, G., Guimond, S., Reiser, J., Peterson, D. A., & Dubey, M. (2021). Contrasting stratospheric smoke mass and lifetime from 2017 Canadian and 2019/2020 Australian megafires: Global simulations and satellite observations [Data set]. <https://doi.org/10.6084/m9.figshare.17056145>
- Das, S., Colarco, P. R., Oman, L. D., Taha, G., & Torres, O. (2021). The long-term transport and radiative impacts of the 2017 British Columbia pyrocumulonimbus smoke aerosols in the stratosphere. *Atmospheric Chemistry and Physics*, 21(15), 12069–12090. <https://doi.org/10.5194/acp-21-12069-2021>
- Ditas, J., Ma, N., Zhang, Y., Assmann, D., Neumaier, M., Riede, H., et al. (2018). Strong impact of wildfires on the abundance and aging of black carbon in the lowermost stratosphere. *Proceedings of the National Academy of Sciences*, 115(50), E11595–E11603. <https://doi.org/10.1073/pnas.1806868115>
- Fasullo, J. T., Rosenbloom, N., Buchholz, R. R., Danabasoglu, G., Lawrence, D. M., & Lamarque, J.-F. (2021). Coupled climate responses to recent Australian wildfire and COVID-19 emissions anomalies estimated in cesm2. *Geophysical Research Letters*, 48(15), e2021GL093841. <https://doi.org/10.1029/2021GL093841>
- Flittner, D., Thomason, L., Hill, C., Roell, M., Pitts, M., Damadeo, R., & Stanley, R. (2018). Stratospheric aerosol and gas experiment III installed on the international space station (SAGE III/ISS): Overview. In *Egu general assembly conference abstracts* (p. 5483).
- Fromm, M. D., Alfred, J., Hoppel, K., Hornstein, J., Bevilacqua, R., Shettle, E., et al. (2000). Observations of boreal forest fire smoke in the stratosphere by POAM III, SAGE II, and lidar in 1998. *Geophysical Research Letters*, 27(9), 1407–1410. <https://doi.org/10.1029/1999GL011200>
- Fromm, M. D., Bevilacqua, R., Servranckx, R., Rosen, J., Thayer, J. P., Herman, J., & Larko, D. (2005). Pyro-cumulonimbus injection of smoke to the stratosphere: Observations and impact of a super blowup in northwestern Canada on 3–4 August 1998. *Journal of Geophysical Research*, 110(D8), D08205. <https://doi.org/10.1029/2004JD005350>
- Fromm, M. D., Kablick, G. P., Peterson, D. A., Kahn, R. A., Flower, V. J. B., & Seftor, C. J. (2021). Quantifying the source term and uniqueness of the August 12, 2017 Pacific northwest PyroCb event. *Journal of Geophysical Research*, 126(13), e34928. <https://doi.org/10.1029/2021JD034928>
- Fromm, M. D., & Servranckx, R. (2003). Transport of forest fire smoke above the tropopause by supercell convection. *Geophysical Research Letters*, 30(10), 1542. <https://doi.org/10.1029/2002GL016820>
- Garofalo, L. A., Pothier, M. A., Levin, E. J. T., Campos, T., Kreidenweis, S. M., & Farmer, D. K. (2019). Emission and evolution of submicron organic aerosol in smoke from wildfires in the Western United States. *ACS Earth and Space Chemistry*, 3(7), 1237–1247. <https://doi.org/10.1021/acsearthspacechem.9b00125>
- Ge, C., Wang, J., Carn, S., Yang, K., Ginoux, P., & Krotkov, N. (2016). Satellite-based global volcanic SO₂ emissions and sulfate direct radiative forcing during 2005–2012. *Journal of Geophysical Research*, 121(7), 3446–3464. <https://doi.org/10.1002/2015JD023134>
- Gent, P. R., Danabasoglu, G., Donner, L. J., Holland, M. M., Hunke, E. C., Jayne, S. R., et al. (2011). The community climate system model version 4. *Journal of Climate*, 24(19), 4973–4991. <https://doi.org/10.1175/2011JCL14083.1>
- Hess, M., Koepke, P., & Schult, I. (1998). Optical properties of aerosols and clouds: The Software package OPAC. *Bulletin of the American Meteorological Society*, 79(5), 831–844. [https://doi.org/10.1175/1520-0477\(1998\)079<0831:OPOAAC>2.0.CO;2](https://doi.org/10.1175/1520-0477(1998)079<0831:OPOAAC>2.0.CO;2)
- Hirsch, E., & Koren, I. (2021). Record-breaking aerosol levels explained by smoke injection into the stratosphere. *Science*, 371(6535), 1269–1274. <https://doi.org/10.1126/science.abe1415>
- Hurrell, J. W., Holland, M. M., Gent, P. R., Ghan, S., Kay, J. E., Kushner, P. J., et al. (2013). The community Earth system model: A framework for collaborative research. *Bulletin of the American Meteorological Society*, 94(9), 1339–1360. <https://doi.org/10.1175/BAMS-D-12-00121.1>
- Jaross, G., Bhartia, P. K., Chen, G., Kowitz, M., Haken, M., Chen, Z., et al. (2014). OMPS Limb profiler instrument performance assessment. *Journal of Geophysical Research*, 119(7), 4399–4412. <https://doi.org/10.1002/2013JD020482>
- Jégou, F., Berthet, G., Brogniez, C., Renard, J.-B., François, P., Haywood, J. M., et al. (2013). Stratospheric aerosols from the Sarychev volcano eruption in the 2009 arctic summer. *Atmospheric Chemistry and Physics*, 13(13), 6533–6552. <https://doi.org/10.5194/acp-13-6533-2013>
- Jolly, W. M., Cochrane, M. A., Freeborn, P. H., Holden, Z. A., Brown, T. J., Williamson, G. J., & Bowman, D. M. J. S. (2015). Climate-induced variations in global wildfire danger from 1979 to 2013. *Nature Communications*, 6(1), 7537. <https://doi.org/10.1038/ncomms8537>
- Jost, H.-J., Drdla, K., Stohl, A., Pfister, L., Loewenstein, M., Lopez, J. P., et al. (2004). In-situ observations of mid-latitude forest fire plumes deep in the stratosphere. *Geophysical Research Letters*, 31(11), L11101. <https://doi.org/10.1029/2003GL019253>

- Kablick, G. P., Allen, D. R., Fromm, M. D., & Nedoluha, G. E. (2020). Australian PyroCb smoke generates synoptic-scale stratospheric anticyclones. *Geophysical Research Letters*, 47(13), e88101. <https://doi.org/10.1029/2020GL088101>
- Kablick, G. P., Fromm, M. D., Miller, S., Partain, P., Peterson, D., Lee, S., et al. (2018). The great slave lake pyrocb of 5 august 2014: Observations, simulations, comparisons with regular convection, and impact on utls water vapor. *Journal of Geophysical Research: Atmospheres*, 123(21), 12332–12352. <https://doi.org/10.1029/2018jd028965>
- Kar, J., Lee, K.-P., Vaughan, M. A., Tackett, J. L., Trepte, C. R., Winker, D. M., et al. (2019). CALIPSO level 3 stratospheric aerosol profile product: Version 1.00 algorithm description and initial assessment. *Atmospheric Measurement Techniques*, 12(11), 6173–6191. <https://doi.org/10.5194/amt-12-6173-2019>
- Kay, J. E., Deser, C., Phillips, A., Mai, A., Hannay, C., Strand, G., et al. (2015). The community Earth system model (CESM) large ensemble project: A community resource for studying climate change in the presence of internal climate variability. *Bulletin of the American Meteorological Society*, 96(8), 1333–1349. <https://doi.org/10.1175/BAMS-D-13-00255.1>
- Khaykin, S., Legras, B., Bucci, S., Sellitto, P., Isaksen, I., Tencé, F., et al. (2020). The 2019/20 Australian wildfires generated a persistent smoke-charged vortex rising up to 35 km altitude. *Communications Earth & Environment*, 1(1), 22. <https://doi.org/10.1038/s43247-020-00022-5>
- Khaykin, S. M., Godin-Beekmann, S., Hauchecorne, A., Pelon, J., Ravetta, F., & Keckhut, P. (2018). Stratospheric smoke with unprecedentedly high backscatter observed by lidars above southern France. *Geophysical Research Letters*, 45(3), 1639–1646. <https://doi.org/10.1002/2017gl076763>
- Kim, M.-H., Omar, A. H., Tackett, J. L., Vaughan, M. A., Winker, D. M., Trepte, C. R., et al. (2018). The CALIPSO version 4 automated aerosol classification and lidar ratio selection algorithm. *Atmospheric Measurement Techniques*, 11(11), 6107–6135. <https://doi.org/10.5194/amt-11-6107-2018>
- Kloss, C., Berthet, G., Sellitto, P., Ploeger, F., Bucci, S., Khaykin, S., et al. (2019). Transport of the 2017 Canadian wildfire plume to the tropics via the Asian monsoon circulation. *Atmospheric Chemistry and Physics*, 19(21), 13547–13567. <https://doi.org/10.5194/acp-19-13547-2019>
- Knepp, T. N., Thomason, L., Roell, M., Damadeo, R., Leavor, K., Leblanc, T., et al. (2020). Evaluation of a method for converting stratospheric aerosol and gas experiment (SAGE) extinction coefficients to backscatter coefficients for intercomparison with lidar observations. *Atmospheric Measurement Techniques*, 13(8), 4261–4276. <https://doi.org/10.5194/amt-13-4261-2020>
- Lack, D. A., & Cappa, C. D. (2010). Impact of brown and clear carbon on light absorption enhancement, single scatter albedo and absorption wavelength dependence of black carbon. *Atmospheric Chemistry and Physics*, 10(9), 4207–4220. <https://doi.org/10.5194/acp-10-4207-2010>
- Lee, J. E., Dubey, M. K., Aiken, A. C., Chylek, P., & Carrico, C. M. (2020). Optical and chemical analysis of absorption enhancement by mixed carbonaceous aerosols in the 2019 Woodbury, AZ, fire plume. *Journal of Geophysical Research*, 125(15), e32399. <https://doi.org/10.1029/2020JD032399>
- Lestrelin, H., Legras, B., Podglajen, A., & Salihoglu, M. (2021). Smoke-charged vortices in the stratosphere generated by wildfires and their behaviour in both hemispheres: Comparing Australia 2020 to Canada 2017. *Atmospheric Chemistry and Physics*, 21(9), 7113–7134. <https://doi.org/10.5194/acp-21-7113-2021>
- Lin, S.-J. (2004). A “vertically Lagrangian” finite-volume dynamical core for global models. *Monthly Weather Review*, 132(10), 2293–2307. [https://doi.org/10.1175/1520-0493\(2004\)132<2293:AVLFDC>2.0.CO;2](https://doi.org/10.1175/1520-0493(2004)132<2293:AVLFDC>2.0.CO;2)
- Liu, D., He, C., Schwarz, J. P., & Wang, X. (2020). Lifecycle of light-absorbing carbonaceous aerosols in the atmosphere. *NPJ Climate and Atmospheric Science*, 3(1), 40. <https://doi.org/10.1038/s41612-020-00145-8>
- Liu, S., Aiken, A. C., Arata, C., Dubey, M. K., Stockwell, C. E., Yokelson, R. J., et al. (2014). Aerosol single scattering albedo dependence on biomass combustion efficiency: Laboratory and field studies. *Geophysical Research Letters*, 41(2), 742–748. <https://doi.org/10.1002/2013GL058392>
- Liu, Z., Vaughan, M., Winker, D., Kittaka, C., Getzewich, B., Kuehn, R., et al. (2009). The CALIPSO lidar cloud and aerosol discrimination: Version 2 algorithm and initial assessment of performance. *Journal of Atmospheric and Oceanic Technology*, 26(7), 1198–1213. <https://doi.org/10.1175/2009JTECHA1229.1>
- Liu, Z., Vaughan, M. A., Winker, D. M., Hostetler, C. A., Poole, L. R., Hlavka, D., & McGill, M. (2004). Use of probability distribution functions for discriminating between cloud and aerosol in lidar backscatter data. *Journal of Geophysical Research*, 109(D15), D15202. <https://doi.org/10.1029/2004JD004732>
- Loughman, R., Bhartia, P. K., Chen, Z., Xu, P., Nyaku, E., & Taha, G. (2018). The ozone mapping and profiler suite (OMPS) limb profiler (LP) version 1 aerosol extinction retrieval algorithm: Theoretical basis. *Atmospheric Measurement Techniques*, 11(5), 2633–2651. <https://doi.org/10.5194/amt-11-2633-2018>
- Malone, R. C., Auer, L. H., Glatzmaier, G. A., Wood, M. C., & Toon, O. B. (1985). Influence of solar heating and precipitation scavenging on the simulated lifetime of post-nuclear war smoke. *Science*, 230(4723), 317–319. <https://doi.org/10.1126/science.230.4723.317>
- Marsh, D. R., Mills, M. J., Kinnison, D. E., Lamarque, J.-F., Calvo, N., & Polvani, L. M. (2013). Climate change from 1850 to 2005 simulated in CESM1(WACCM). *Journal of Climate*, 26(19), 7372–7391. <https://doi.org/10.1175/JCLI-D-12-00558.1>
- McCormick, M. P., Thomason, L. W., & Trepte, C. R. (1995). Atmospheric effects of the Mt Pinatubo eruption. *Nature*, 373(6513), 399–404. <https://doi.org/10.1038/373399a0>
- McCormick, M. P., & Veiga, R. E. (1992). SAGE II measurements of early Pinatubo aerosols. *Geophysical Research Letters*, 19(2), 155–158. <https://doi.org/10.1029/91GL02790>
- Meinshausen, M., Smith, S. J., Calvin, K., Daniel, J. S., Kainuma, M. L. T., Lamarque, J.-F., et al. (2011). The RCP greenhouse gas concentrations and their extensions from 1765 to 2300. *Climatic Change*, 109(1), 213–241. <https://doi.org/10.1007/s10584-011-0156-z>
- Mills, M. J., Toon, O. B., Lee-Taylor, J., & Robock, A. (2014). Multidecadal global cooling and unprecedented ozone loss following a regional nuclear conflict. *Earth's Future*, 2(4), 161–176. <https://doi.org/10.1002/2013EF000205>
- Minnis, P., Harrison, E. F., Stowe, L. L., Gibson, G. G., Denn, F. M., Doelling, D. R., et al. (1993). Radiative climate forcing by the Mount Pinatubo eruption. *Science*, 259(5100), 1411–1415. <https://doi.org/10.1126/science.259.5100.1411>
- Murphy, D. M., Froyd, K. D., Bourgeois, I., Brock, C. A., Kupe, A., Peischl, J., et al. (2021). Radiative and chemical implications of the size and composition of aerosol particles in the existing or modified global stratosphere. *Atmospheric Chemistry and Physics*, 21(11), 8915–8932. <https://doi.org/10.5194/acp-21-8915-2021>
- Nolan, R. H., Boer, M. M., Collins, L., Resco de Dios, V., Clarke, H., Jenkins, M., et al. (2020). Causes and consequences of eastern Australia's 2019-20 season of mega-fires. *Global Change Biology*, 26(3), 1039–1041. <https://doi.org/10.1111/gcb.14987>
- Ohneiser, K., Ansmann, A., Baars, H., Seifert, P., Barja, B., Jimenez, C., et al. (2020). Smoke of extreme Australian bushfires observed in the stratosphere over punta arenas, Chile, in January 2020: Optical thickness, lidar ratios, and depolarization ratios at 355 and 532 nm. *Atmospheric Chemistry and Physics*, 20(13), 8003–8015. <https://doi.org/10.5194/acp-20-8003-2020>
- Omar, A. H., Winker, D. M., Kittaka, C., Vaughan, M. A., Liu, Z., Hu, Y., et al. (2009). The CALIPSO automated aerosol classification and lidar ratio selection algorithm. *Journal of Atmospheric and Oceanic Technology*, 26(10), 1994–2014. <https://doi.org/10.1175/2009JTECHA1231.1>

- Omar, A. H., Won, J.-G., Winker, D. M., Yoon, S.-C., Dubovik, O., & McCormick, M. P. (2005). Development of global aerosol models using cluster analysis of Aerosol Robotic Network (AERONET) measurements. *Journal of Geophysical Research*, 110(D10), D10S14. <https://doi.org/10.1029/2004JD004874>
- Parks, S. A., & Abatzoglou, J. T. (2020). Warmer and drier fire seasons contribute to increases in area burned at high severity in Western us forests from 1985 to 2017. *Geophysical Research Letters*, 47(22), e89858. <https://doi.org/10.1029/2020gl089858>
- Peterson, D. A., Campbell, J. R., Hyer, E. J., Fromm, M. D., Kablick, G. P., Cossuth, J. H., & DeLand, M. T. (2018). Wildfire-driven thunderstorms cause a volcano-like stratospheric injection of smoke. *NPJ Climate and Atmospheric Science*, 1(1), 30. <https://doi.org/10.1038/s41612-018-0039-3>
- Peterson, D. A., Fromm, M. D., McRae, R. H. D., Campbell, J. R., Hyer, E. J., Taha, G., et al. (2021). Australia's black summer pyrocumulonimbus super outbreak reveals potential for increasingly extreme stratospheric smoke events. *NPJ Climate and Atmospheric Science*, 4(1), 38. <https://doi.org/10.1038/s41612-021-00192-9>
- Peterson, D. A., Hyer, E. J., Campbell, J. R., Solbrig, J. E., & Fromm, M. D. (2017). A conceptual model for development of intense pyrocumulonimbus in Western North America. *Monthly Weather Review*, 145(6), 2235–2255. <https://doi.org/10.1175/MWR-D-16-0232.1>
- Pumphrey, H. C., Schwartz, M. J., Santee, M. L., Kablick, I., George, P., Fromm, M. D., & Livesey, N. J. (2021). Microwave limb sounder (MLS) observations of biomass burning products in the stratosphere from Canadian forest fires in August 2017. *Atmospheric Chemistry and Physics*, 21(22), 16645–16659. <https://doi.org/10.5194/acp-21-16645-2021>
- Rault, D. F., & Loughman, R. P. (2013). The OMPS limb profiler environmental data record algorithm theoretical basis document and expected performance. *IEEE Transactions on Geoscience and Remote Sensing*, 51(5), 2505–2527. <https://doi.org/10.1109/TGRS.2012.2213093>
- Rienecker, M. M., Suarez, M. J., Todling, R., Bacmeister, J., Takacs, L., Liu, H.-C., & Nielsen, J. (2008). *The geos-5 data assimilation system - documentation of versions 5.0.1, 5.1.0, and 5.2.0*. (Tech. Rep. No. 27). NASA Goddard Space Flight Center report.
- Romonosky, D. E., & Gomez, S. L. (2019). Optical properties of laboratory and ambient biomass burning aerosols: Elucidating black, brown, and organic carbon components and mixing regimes. *Journal of Geophysical Research*, 124(9), 5088–5105. <https://doi.org/10.1029/2018JD029892>
- Schallock, J., Brühl, C., Bingen, C., Höpfner, M., Rieger, L., & Lelieveld, J. (2021). Radiative forcing by volcanic eruptions since 1990, calculated with a chemistry-climate model and a new emission inventory based on vertically resolved satellite measurements. *Atmospheric Chemistry and Physics Discussions*, 2021, 1–38. <https://doi.org/10.5194/acp-2021-654>
- Schmidt, A., Mills, M. J., Ghan, S., Gregory, J. M., Allan, R. P., Andrews, T., et al. (2018). Volcanic radiative forcing from 1979 to 2015. *Journal of Geophysical Research*, 123(22), 12491–12508. <https://doi.org/10.1029/2018JD028776>
- Schwartz, M. J., Santee, M. L., Pumphrey, H. C., Manney, G. L., Lambert, A., Livesey, N. J., et al. (2020). Australian New year's PyroCb impact on stratospheric composition. *Geophysical Research Letters*, 47(24), e90831. <https://doi.org/10.1029/2020GL090831>
- Self, S., Zhao, J.-X., Holasek, R., Torres, R., & King, A. (1998). The atmospheric impact of the 1991 Mount Pinatubo eruption. In C. Newhall, & R. Punongbayan (Eds.), *Fire and mud, eruptions and lahars of mount pinatubo, Philippines*.
- Shiraishi, T., & Hirata, R. (2021). Estimation of carbon dioxide emissions from the megafires of Australia in 2019–2020. *Scientific Reports*, 11(1), 8267. <https://doi.org/10.1038/s41598-021-87721-x>
- Simpson, J. I., Akagi, S. K., Barletta, B., Blake, N. J., Choi, Y., Diskin, G. S., et al. (2011). Boreal forest fire emissions in fresh Canadian smoke plumes: C₁-C₁₀ volatile organic compounds (VOCs), CO₂, CO, NO₂, NO, HCN and CH₃CN. *Atmospheric Chemistry and Physics*, 11(13), 6445–6463. <https://doi.org/10.5194/acp-11-6445-2011>
- Solomon, S., Dube, K., Stone, K., Yu, P., Kinnison, D., Toon, O. B., et al. (2022). On the stratospheric chemistry of midlatitude wildfire smoke. *Proceedings of the National Academy of Sciences*, 119(10), e2117325119. <https://doi.org/10.1073/pnas.2117325119>
- Stenke, A., Hoyle, C. R., Luo, B., Rozanov, E., Gröbner, J., Maag, L., et al. (2013). Climate and chemistry effects of a regional scale nuclear conflict. *Atmospheric Chemistry and Physics*, 13(19), 9713–9729. <https://doi.org/10.5194/acp-13-9713-2013>
- Stephens, G. L., Vane, D. G., Boain, R. J., Mace, G. G., Sassen, K., Wang, Z., et al. (2002). The cloudsat mission and the A-train. *Bulletin of the American Meteorological Society*, 83(12), 1771–1790. <https://doi.org/10.1175/BAMS-83-12-1771>
- Stowe, L. L., Carey, R. M., & Pellegrino, P. P. (1992). Monitoring the Mt. Pinatubo aerosol layer with NOAA/11 AVHRR data. *Geophysical Research Letters*, 19(2), 159–162. <https://doi.org/10.1029/91GL02958>
- Taha, G., Loughman, R., Zhu, T., Thomason, L., Kar, J., Rieger, L., & Bourassa, A. (2021). OMPS LP Version 2.0 multi-wavelength aerosol extinction coefficient retrieval algorithm. *Atmospheric Measurement Techniques*, 14(2), 1015–1036. <https://doi.org/10.5194/amt-14-1015-2021>
- Taylor, K. E., Stouffer, R. J., & Meehl, G. A. (2012). An Overview of CMIP5 and the experiment design. *Bulletin of the American Meteorological Society*, 93(4), 485–498. <https://doi.org/10.1175/BAMS-D-11-00094.1>
- Torres, O., Bhartia, P. K., Taha, G., Jethva, H., Das, S., Colarco, P., et al. (2020). Stratospheric injection of massive smoke plume from Canadian boreal fires in 2017 as seen by DSCOVR-EPIC, CALIOP, and OMPS-LP observations. *Journal of Geophysical Research*, 125(10), e32579. <https://doi.org/10.1029/2020JD032579>
- Valero, F. P. J., & Pilewskie, P. (1992). Latitudinal survey of spectral optical depths of the Pinatubo volcanic cloud-derived particle sizes, columnar mass loadings, and effects on planetary albedo. *Geophysical Research Letters*, 19(2), 163–166. <https://doi.org/10.1029/92GL00074>
- Wang, J., Park, S., Zeng, J., Ge, C., Yang, K., Carn, S., et al. (2013). Modeling of 2008 Kasatochi volcanic sulfate direct radiative forcing: Assimilation of OMI SO₂ plume height data and comparison with MODIS and CALIOP observations. *Atmospheric Chemistry and Physics*, 13(4), 1895–1912. <https://doi.org/10.5194/acp-13-1895-2013>
- Westerling, A. L. (2016). Increasing Western US forest wildfire activity: Sensitivity to changes in the timing of spring. *Philosophical Transactions of the Royal Society B: Biological Sciences*, 371(1696). <https://doi.org/10.1098/rstb.2015.0178>
- Winker, D. M., Pelon, J. R., & McCormick, M. P. (2003). The CALIPSO mission: Spaceborne lidar for observation of aerosols and clouds. *Society of photo-optical instrumentation engineers (Spie) conference Series* (Vol. 4893, pp. 1–11). <https://doi.org/10.1117/12.466539>
- Winker, D. M., Vaughan, M. A., Omar, A., Hu, Y., Powell, K. A., Liu, Z., et al. (2009). Overview of the CALIPSO mission and CALIOP data processing algorithms. *Journal of Atmospheric and Oceanic Technology*, 26(11), 2030–2323. <https://doi.org/10.1175/2009JTECHA1281.1>
- Yee, L. D., Kautzman, K. E., Loza, C. L., Schilling, K. A., Coggon, M. M., Chhabra, P. S., et al. (2013). Secondary organic aerosol formation from biomass burning intermediates: Phenol and methoxyphenols. *Atmospheric Chemistry and Physics*, 13(16), 8019–8043. <https://doi.org/10.5194/acp-13-8019-2013>
- Yu, P., Davis, S. M., Toon, O. B., Portmann, R. W., Bardeen, C. G., Barnes, J. E., et al. (2021). Persistent stratospheric warming due to 2019–2020 Australian wildfire smoke. *Geophysical Research Letters*, 48(7), e92609. <https://doi.org/10.1029/2021GL092609>
- Yu, P., Toon, O. B., Bardeen, C. G., Zhu, Y., Rosenlof, K. H., Portmann, R. W., et al. (2019). Black carbon lifts wildfire smoke high into the stratosphere to form a persistent plume. *Science*, 365(6453), 587–590. <https://doi.org/10.1126/science.aax1748>